

This is to certify that the

thesis entitled

EXPERIMENTAL VERIFICATION OF PROPER ORTHOGONAL DECOMPOSITION IN A CANTILEVER BEAM

presented by

Muhammad Saqib Riaz

has been accepted towards fulfillment
of the requirements for

MS
Mechanical Engineering
degree in

PROF. BRIAN F. FEENY

Major professor

Date Sept. 22, 2000

MSU is an Affirmative Action/Equal Opportunity Institution

0-7639

LIBRARY Michigan State University

PLACE IN RETURN BOX to remove this checkout from your record. TO AVOID FINES return on or before date due. MAY BE RECALLED with earlier due date if requested.

DATE DUE	DATE DUE	DATE DUE
JAN 1 2 2009		

11/00 c/CIRC/DateDue.p85-p.14

Experimental Verification of Proper Orthogonal Decomposition in a Cantilever Beam

Ву

Muhammad Saqib Riaz

A THESIS

Submitted to
Michigan State University
in partial fulfillment of the requirements
for the degree of

MASTER OF SCIENCE

Department of Mechanical Engineering

2000

Professor Brian F. Feeny

ABSTRACT

Experimental Verification of Proper Orthogonal Decomposition in a Cantilever Beam

By

Muhammad Saqib Riaz

We apply proper orthogonal decomposition (POD) to an experimental system, which results in a set of proper orthogonal modes (POMs) and proper orthogonal values. The experiments were performed using a cantilever beam, excited by an impulse input and sensed with strain gages. The strains were converted to displacements and POD was performed on the displacements. The experimental setup matched conditions under which, according to vibration theory, the POMs should approximately converge to the linear normal modes. The POMs were compared with the theoretical normal modes. The results confirmed the validity of this method for acquiring lower modes of vibration. To study the robustness of the method, we examined the effect of changing data acquisition parameters such as sampling rate, number of samples and time record, and we applied input at different locations on the cantilever. We also used different types of basis functions for converting strains to displacements.

į

1

|

To my parents & my family

ACKNOWLEDGEMENTS

During my stay at MSU, I have obtained a great deal of valuable academic and non-academic assistance from a lot of generous people like Dr Brian Feeny. The interaction between us gave me, not only a high level of academic knowledge, but also provided me a chance to work with a wonderful person. I would like to thank him for his technical and financial help and giving me freedom to work, so that I can practice my own ideas and gain technical confidence.

Dr Alan Haddow deserves special thanks for his guidance and encouragement in all the steps of my work. I am also indebted to Dr Steven Shaw, who taught, and helped me in building my basics in the field of vibrations. It is my most humble duty to thank all my teachers at National University of Sciences and Technology, Pakistan, who taught and encouraged me to reach this point. Dr Khurshid Zaidi, Dr Aafzal Malik, Dr Rafique and Dr Akhter Nawaz deserve a special mention in this connection. I would like to thank all the members of Dynamics laboratory, whose association was a continuous help in keeping my spirits high.

Contents

1	Introduction 1		1
	1.1	Thesis statement	.1
	1.2	Background	. 1
	1.3	Motivation	4
	1.4	Proposed Research	5
	1.5	Contribution	5
	1.6	Thesis organization	6
2	Modal 7	Testing Procedure	7
	2.1	Definition and theory	.7
	2.2	POD for discrete linear systems	.10
	2.3	POD for distributed linear systems	.12
	2.4	Conventional Modal Analysis	15
3	Experin	nental Setup	18
	3.1	Beam Model	.18
	3.2	Physical Beam	.19
	3.3	Strain gages and instrumentation	.21
	3.4	Voltage to strain	.22

6	Bibli	ography	83
	5.3	Future Work	.81
	5.2	Conclusions	.78
	5.1	Summary of work	77
5	Conclu	sion	77
	4.6	POD with Admissible Basis functions	.62
	4.5	POMs based on a large number of "pseudo sensors"	.57
		4.4.2 Experimentation and results	.53
		4.4.1 Strain Modes	51
	4.4	Decomposition of the strain signals	51
	4.3	POD with variable time record length	45
	4.2	POD with input at various points of the system	39
	4.1	POD with variable sampling rate	32
4	Tests a	nd Results	31
	3.6	Identification of modal frequencies and damping factors	25
	3.5	Strain to displacement	.24

List of Figures

- 3.1 Cantilever beam with strain gages. The beam displacement is normal to the page.
- 3.2 Block diagram showing data acquisition process
- 3.3 Resistances forming "half wheat-stone bridge circuit" configured for bending.
- 3.4 Comparison between theoretical and experimental frequencies of cantilever beam.
- 3.5 Illustration of the calculations of damping ratios by using quadrature peak picking method for lightly damped systems
- 4.1 Proper orthogonal modes with sampling rate of 100 samples per second.
- 4.2 Proper orthogonal modes with sampling rate of 400 samples per second
- 4.3 Proper orthogonal modes with sampling rate of 800 samples per second
- 4.4 Proper orthogonal modes with sampling rate of 1000 samples per second
- 4.5 Proper orthogonal modes with sampling rate of 800 samples per second and force applied between 4th and 5th strain gage.
- 4.6 Proper orthogonal modes with sampling rate of 800 samples per second and force applied between 3rd and 4th strain gage.
- 4.7 Proper orthogonal modes with sampling rate of 800 samples per second and force applied between 2nd and 3rd strain gage.
- 4.8 Proper orthogonal modes with sampling rate of 800 samples per second and force applied between 1st and 2nd strain gage.
- 4.9 Proper orthogonal modes with sampling rate of 800 samples per second and time record length of 0.0075sec. (6 samples)
- 4.10 Proper orthogonal modes with sampling rate of 800 samples per second and time record length of 0.025 sec. (20 samples)
- 4.11 Proper orthogonal modes with sampling rate of 800 samples per second and time record length of 0.25 seconds. (200 samples)

- 4.12 Proper orthogonal modes with sampling rate of 800 samples per second and time record length of 0.5 seconds. (400 samples)
- 4.13 Strain distribution along the length of beam
- 4.14 Displacement modes converted from strain modes with sampling rate of 800 samples per second and input applied between 3rd and 4th strain gage.
- 4.15 Displacement modes converted from strain modes with sampling rate of 800 samples per second and input applied between 3rd and 4th strain gage for zero end strain correlation vectors.
- 4.16 Proper orthogonal modes with sampling rate of 800 samples per second and input applied between 4th and 5th strain gage using 21 pseudo sensors.
- 4.17 Proper orthogonal modes with sampling rate of 800 samples per second and input applied between 3rd and 4th strain gage using 21 pseudo sensors.
- 4.18 Proper orthogonal modes with sampling rate of 800 samples per second and input applied between 2nd and 3rd strain gage using 21 pseudo sensors.
- 4.19 Proper orthogonal modes with sampling rate of 800 samples per second using 1st set of admissible functions. (-- show the LNMs)
- 4.20 Proper orthogonal modes with sampling rate of 1000 samples per second using 1st set of admissible functions. (-- show the LNMs)
- 4.21 Proper orthogonal modes with sampling rate of 800 samples per second using 1st set of admissible functions. (-- show the Basis functions)
- 4.22 Proper orthogonal modes with sampling rate of 800 samples per second using 1st set of admissible functions with 21 pseudo sensors

- 4.23 Proper orthogonal modes with sampling rate of 1000 samples per second using 1st set of admissible functions with 21 pseudo sensors
- 4.24 Proper orthogonal modes with sampling rate of 800 samples per second using 1st set of admissible functions with 41 pseudo sensors
- 4.25 Proper orthogonal modes with sampling rate of 800 samples per second using 2nd set of admissible functions.
- 4.26 Proper orthogonal modes with sampling rate of 1000 samples per second using 2nd set of admissible functions.
- 4.27 Proper orthogonal modes with sampling rate of 800 samples per second using 2nd set of admissible functions with 21 pseudo sensors
- 4.28 Proper orthogonal modes with sampling rate of 1000 samples per second using 2nd set of admissible functions with 21 pseudo sensors

List of Tables

- 3.1 Experimental values of time constant and settling time for each mode.
- 3.2 List of node points for the first six linear normal modes of a cantilever beam, measured in x from the fixed end.
- 4.1 Norm of error with LNMs for each mode and their corresponding proper orthogonal values for sampling rate of 100 samples per second.
- 4.2 Norm of error with LNMs for each mode and their corresponding proper orthogonal values for sampling rate of 400 samples per second.
- 4.3 Norm of error with LNMs for each mode and their corresponding proper orthogonal values for sampling rate of 800 samples per second.
- 4.4 Norm of error with LNMs for each mode and their corresponding proper orthogonal values for sampling rate of 1000 samples per second.
- 4.5 Norm of error with LNMs for each mode and their corresponding proper orthogonal values for sampling rate of 800 samples per second.
- 4.6 Norm of error with LNMs for each mode and their corresponding proper orthogonal values for sampling rate of 800 samples per second.
- 4.7 Norm of error with LNMs for each mode and their corresponding proper orthogonal values for sampling rate of 800 samples per second.
- 4.8 Norm of error with LNMs for each mode and their corresponding proper orthogonal values for sampling rate of 800 samples per second.
- 4.9 Norm of error with LNMs for each mode and their corresponding proper orthogonal values for sampling rate of 800 samples per second.

- 4.10 Norm of error with LNMs for each mode and their corresponding proper orthogonal values for sampling rate of 800 samples per second.
- 4.11 Norm of error with LNMs for each mode and their corresponding proper orthogonal values for sampling rate of 800 samples per second.
- 4.12 Norm of error with LNMs for each mode and their corresponding proper orthogonal values for sampling rate of 800 samples per second.
- 4.13 Norm of error with linear normal modes for each mode and their corresponding strain POVs for sampling rate of 800 samples per second.
- 4.14 Norm of error with linear normal modes for each mode and their corresponding strain POVs for sampling rate of 800 samples per second.
- 4.15 Norm of error with 1st set of admissible functions for each mode and their corresponding proper orthogonal values for sampling rate of 800 samples/sec.
- 4.16 Norm of error with 1st set of admissible functions for each mode and their corresponding proper orthogonal values for sampling rate of 1000 samples/sec.
- 4.17 Norm of error with 1st set of admissible functions for each mode and their corresponding proper orthogonal values for sampling rate of 800 samples/sec.
- 4.18 Norm of error with 2nd set of admissible functions for each mode and their corresponding proper orthogonal values for sampling rate of 800 samples/ sec.
- 4.19 Norm of error with 2nd set of admissible functions for each mode and their corresponding proper orthogonal values for sampling rate of 1000 samples/ sec.

Chapter 1

Introduction

1.1 Thesis statement

Recent studies have shown that under certain circumstances, proper orthogonal modes (POMs) make good approximations to linear normal modes. While such studies have been theoretical and numerical, no controlled experiments have been performed in this field. The goal of this thesis is to experimentally verify that POMs approximate linear normal modes under appropriate conditions.

1.2 Background

Proper orthogonal decomposition (POD) is an experimental technique which can be used to find the energy modes of vibrations and optimal energy distribution in a system. POD is emerging as a useful experimental tool in dynamics and vibrations. Real systems are often non-linear for even simple geometries. The attraction of POD lies in the fact that it is a linear procedure. "This robustness makes it a safe haven in the intimidating world of non-linearity" [3]. In other disciplines the same procedure was used with different names, such as Karhunen-Loève decomposition and principal components analysis, and it seems to have been independently rediscovered many times.

Lumley [3,18,19] traced this idea back to independent investigations by Kosambi (1943), Loève (1945), Karhunen (1946), Pogachev (1953), and Obukhov (1954). POD is closely related to the principal component analysis (PCA) and singular value decomposition (SVD) according to Ravindra [11]. Beltrami introduced SVD for the first time in 1873 and subsequently Jordan (1874), Sylvester (1889), Schimdt (1907) and Weyl (1912) developed the method further.

The method is used in a number of fields as turbulence, vibration analysis, image processing, signal analysis, data compression, process identification and control in chemical engineering. In the field of mechanics, Lumley [3,18,19] first explored this technique in the 1960's in understanding coherent structures of turbulent flows.

The application of POD to structures started few years ago. Cusumano and Bai [6] and Cusumano et al. [7] used POD for the estimation of number of active states in chaotic attractors. FitzSimons and Rui [8] used it for understanding of the modal distribution systems and applied it to modal reduction. More recently Murphy [9] applied this technique on understanding snap-through oscillations of buckled plates. Sipcic et al. [10] used it for investigation of fluid/structure interaction problems. Feeny [1,2] and Kappagantu [1,5] worked on interpreting the proper orthogonal modes in vibrations. Davies and Moon [14] applied POD to a nonlinear periodic structure, and noticed correlation between POMs and linear normal modes. Yasuda and Kamiya [17] employed an equivalent method to uncover modes to be used for nonlinear system identification. Azeez and Vakakis [15] used Karhunen-Loève decomposition to analyze the vibroimpact

response for a rotor. Ma et al. [16] used POD for the identification of nonparametric, nonlinear system identification of a nonlinear flexible system. The level of accuracy achieved by researchers was different for different applications.

The related SVD has also been widely used for example in the case of substructuring problems in structural dynamics and modal analysis [12]. In these cases SVD has been found an effective and reliable tool in solving rank deficiency and modal reduction and noise reduction problems. SVD is a frequently used tool to compute the number of active degree of freedom or order of the model in system identification [13].

Feeny and Kappagantu [1] proved theoretically that the POMs converge to the linear normal modes in discrete structures with a known mass distribution, in the case of undamped free vibration, lightly damped and forced vibrations. They also showed that the POMs represent the principal axes of inertia of the data in the measurement space. For the case of a synchronous non-linear normal mode, the dominant POM provides a best fit of the normal mode. Feeny [2] extended the above idea to continuous systems. He showed that if the distributed system is discretized evenly, POMs approximate the linear normal modes. He applied this to a cantilever and on a hinged-hinged beam numerically. B. Ravindra [11] added to the discussion on POD by Feeny and Kappagantu [1] and tried to point out potential problems with these estimations.

1.3 Motivation

All mechanical systems can be viewed as continuous systems. Due to infinite dimensionality, continuous systems can be difficult to analyze. Generally continuous systems are described by partial differential equations (PDEs). Analytical solution to these governing equations may not be available and boundary conditions may not be well specified. An approach to tackling continuous systems is to identify modes, and use them to project the system to a lower-order model. In the field of structures modal analysis, mode extraction and characterization from real vibrating system has always been a challenging task. Modal analysis is a form of nonparametric system identification, as it helps in recognizing degrees of freedom and associated properties. It provides us a basis for transformation from physical coordinates to natural modal coordinates.

Traditional modal analysis requires frequency response measurements with several combinations of input and output locations, whereas POD requires a single set of time histories from several output locations. However, more system information is often needed to interpret results. Typical usage of POD has been geared towards nonlinear random or chaotic response. A clean connection with linear systems is worthwhile both in its own rite as well as in interpreting nonlinear results. POD effectively extracts modes in the sense of optimal energy distribution of the system and concentrate more on those modes, which contain maximum energy of the system. These energy modes have been treated as "empirical" modes, which can be used in modal reduction. The POD process enables the optimal distribution of energy to be used as basis.

POD is a linear process and it does not involve any assumption about the linearity of the system. POMs have been shown theoretically to approximate linear modes under certain conditions. A number of numerical simulations have supported this method. So some controlled experiments are needed to check the feasibility of this process experimentally. Thus we are motivated to apply this idea experimentally to systems which meet the requirements, such as lightly damped, linear systems with known mass distribution, to check the performance of this method. This research on the development of POD is warranted to broaden its application in experimental and theoretical contexts.

1.4 Proposed Research

The hypothesis for this research is "the experimental proper orthogonal modes represent the natural modes of vibration for a linear system with a known mass distribution and the experimental proper orthogonal values gives us the distribution of energy in the system". We perform a series of experiments to verify the POD procedure as a tool for estimating normal modes.

1.5 Contributions

The main contribution of this thesis is the verification of the POD procedure experimentally as a modal analysis tool for a class of continuous systems. This method is simple to implement and easy to learn as compared to traditional modal analysis procedures. Thus, it provides experimentalists with a new option for modal analysis of systems in this class.

1.6 Thesis Organization

In the second chapter a discussion about the modal testing procedure, with details on theory and its application on discrete and distributed linear systems is available. It also describes the whole process from data handling to POM extraction. The third chapter provides details about experimental set up and different software and hardware used in experiments. We also discuss the handling of the signals, from voltage to strain and then to displacement. The process of getting properties of our cantilever beam experimentally and theoretically is described in this section. In the fourth chapter we discuss different tests performed and the results obtained form them. In order to increase resolution of our results, we used a redundant set of pseudo displacements. We also used different sets of admissible functions for a cantilever beam and compared resulting modes obtained when using those functions as sets of basis functions. In the fifth chapter we conclude with a summary of the overall results and indicate the direction of the future work.

Chapter 2

Modal Testing Procedure

In this chapter we will discuss the theory of proper orthogonal decomposition and will see the application of this to the linear normal modes. We will also go through the application of this method to continuous systems, taking a simple example of a cantilever beam. We restrict our studies to linear systems only.

2.1 Definition and theory

From vibration point of view, two important quantities that can be obtained experimentally are the system's natural frequencies and associated mode shapes. The mode shape is the shape in which a system vibrates synchronously at, or close to, its natural frequency. There are conventional methods used for determining these properties. The most important assumption regarding those methods is that the system under test is linear and is driven by the test input only in its linear range. POD does not require the assumption of linearity of the system. However, linearity must be assumed if the POMs are to be tied to linear normal modes.

Determining the mode shapes from experimentally measured transfer functions is slightly more complicated and involves the measurement of several transfer functions [4]. The POD procedure is simple and involves fewer computations. So we prefer POD, due to its simplicity and linearity, to other conventional methods. However, POD is only applicable as a modal analysis tool if the mass distribution is known.

During the experimentation process of finding various modes for our cantilever, we tried to apply a conventional method discussed by Inman [4], which requires impulses at several locations of the beam to produce frequency response associated with inputs at those locations. Our beam was so floppy that we could not generate a meaningful signal on the impulse hammer. This points to an advantage of the POD method, for which multiple input locations are not generally required at least for obtaining mode shapes. We will discuss this in detail in Chapter 3.

As noted above, in order to describe mode shapes in the displacement coordinate, the mass matrix must be known. Thus there is a trade off between POD and conventional modal analysis in terms of information gathering. In lieu of determining the mass distribution, the conventional method requires several impulse responses, and records of the input signals.

More generally the POD procedure is a simple experimental technique used for evaluating the spatial properties of a system. It has been applied to turbulent flows and image processing, and more recently to dynamic structures. In statistical studies we imagine that the same experiment is performed repeatedly and the value of the quantity is recorded. This method requires measurement or knowledge of some numerical values, e.g. displacements along of the beam during the course of time, resulting in a large number of data under superficially identical conditions. We call this set of data an ensemble. This ensemble is then used to make a correlation matrix, whose eigenvalues and eigenvectors give us the proper orthogonal modes and proper orthogonal values. These quantities mean different parameters for different applications. Basically this method describes the distribution of energy of a system.

Application of POD to structures requires the sensed displacements of a dynamic system at 'M' locations. Let us call these displacements

$$X_1(t), X_2(t), X_3(t), \dots, X_M(t)$$

If we sample the displacements N times we can form a set of displacement histories

$$\mathbf{x}_{i}(t) = [X_{i}(t_{1}), X_{i}(t_{2}), X_{i}(t_{3}), \dots, X_{i}(t_{N})]^{T}$$
 $i = 1, 2, \dots, M$

In proper orthogonal decomposition we use these set of data to form an N×M ensemble matrix, say

$$X = [x_1, x_2, x_3, x_4, ..., x_M]$$

In the above matrix we have arranged the displacements such that each row represents the displacements of M points at any instant of time. We can make a correlation matrix as $\mathbf{R} = (1/N) \mathbf{X}^T \mathbf{X}$. Since \mathbf{R} is a real and symmetric, its eigenvalues form an orthogonal basis. The eigenvectors of \mathbf{R} are the proper orthogonal modes (POMs) and the eigenvalues of \mathbf{R} are proper orthogonal values (POVs). These POVs indicate the signal

energy associated with the corresponding mode [2], so we can easily find the dominant modes from the energy perspective.

2.2 POD for discrete linear systems

In this section we discuss the application of POD to an unforced, undamped linear multidegree-of-freedom system [2], with positive definite mass and stiffness matrices M and K. The equation of motion for this class of problem is

$$\mathbf{M}\ddot{\mathbf{x}} + \mathbf{K}\mathbf{x} = \mathbf{0} \tag{1}$$

where \mathbf{x} is an M×1 vector of displacements. The modal vectors \mathbf{v}_i , when normalized with respect to the mass matrix, satisfy the orthogonality condition as \mathbf{v}_i^T M $\mathbf{v}_j = \delta_{ij}$ for all i, j = 1, 2, ..., M. A coordinate transformation $\mathbf{x} = \mathbf{M}^{-1/2}\mathbf{q}$ can be made, such that

$$\ddot{\mathbf{q}} + \mathbf{M}^{-1/2}\mathbf{K} \ \mathbf{M}^{-1/2}\mathbf{q} = 0$$

The advantage of this representation is this that its matrices are still symmetric and effective mass matrix is the identity. To this end, we consider equation (1), with $\mathbf{M} = \mathbf{I}$, the orthogonality condition will be $\mathbf{v}_i^T \ \mathbf{v}_j = \delta_{ij}$ Suppose the vibration in the system consists of several modes. We can express motion in general as

 $\mathbf{x}(t) = \mathbf{A}_1 \sin{(\omega_1 t - \varnothing_1)} \mathbf{v}_1 + \mathbf{A}_2 \sin{(\omega_2 t - \varnothing_2)} \mathbf{v}_2 + ... + \mathbf{A}_M \sin{(\omega_M t - \varnothing_M)} \mathbf{v}_M$ where the components of $\mathbf{x}(t)$ are the displacement of particular coordinate, \mathbf{v}_i are the modal vectors and \mathbf{A}_i and \varnothing_i depend upon the initial conditions. The above equation can be rewritten as

$$\mathbf{x}(t) = \mathbf{e}_1(t) \mathbf{v}_1 + \mathbf{e}_2(t) \mathbf{v}_2 + ... + \mathbf{e}_M(t) \mathbf{v}_M$$

where $e_i(t)$ (i = 1, 2, ..., M) are time modulations. Then we can write the X matrix as

$$X = [x_1...x_M]^T = [e_1 v_1^T + ... + e_M v_M^T]$$

Where e_i are the $e_i(t)$ evaluated at the sample times $t = t_1, t_2, t_3, ..., t_N$ to form N×1 vectors. It can be easily checked whether a modal vector is actually a POM by post multiplying the matrix \mathbf{R} by that modal vector. Thus

$$\mathbf{R} \ \mathbf{v}_{j} = \frac{1}{N} \mathbf{X}^{T} \mathbf{X} = \frac{1}{N} \left[\mathbf{e}_{1} \ \mathbf{v}_{1}^{T} + ... + \mathbf{e}_{M} \ \mathbf{v}_{M}^{T} \right]^{T} \left[\mathbf{e}_{1} \ \mathbf{v}_{1}^{T} + ... + \mathbf{e}_{M} \ \mathbf{v}_{M}^{T} \right] \mathbf{v}_{j}$$

Using the orthogonality condition $\mathbf{v}_{i}^{T} \mathbf{v}_{j} = \delta_{ij}$

$$\mathbf{R} \ \mathbf{v}_{j} = \frac{1}{N} \mathbf{X}^{T} \mathbf{X} = \frac{1}{N} [\mathbf{v}_{1}^{T} \mathbf{e}_{1}^{T} \mathbf{e}_{j} + ... + \mathbf{v}_{M}^{T} \mathbf{e}_{M}^{T} \mathbf{e}_{j}]$$

As long as the frequencies of the modes are distinct, each term $\mathbf{v}_i^T \mathbf{e}_i^T \mathbf{e}_j^T \mathbf{e}_j^T$

Feeny and Kappagantu [1] related the normal modes to POMS using numerical and analytical methods on simple mass-spring-damper (MSD) systems. They showed for undamped systems that error decreases with increasing number of samples and time record lengths. For systems with proportional damping and possessing synchronous

modes, they observed the POMs tending towards eigenvectors of the system with increasing number of samples. But the error increases for systems with high damping. In general, POMs lie on the principal axes of inertia of the data in the measurement space. For the case of synchronous nonlinear normal modes, the dominant POM represents a best fit of the nonlinear normal mode. Observations of Ma at el. [16] suggest that this may carry over to oscillations with multiple nonlinear normal modes involved.

2.3 POD for distributed linear systems

In this section we summarize the application of the POD to distributed parameter linear systems [2]. Consider as an example a beam of length L. The unforced model of the system is

$$m(x)\ddot{y} + L_1 y = 0$$

where y(x,t) is a displacement, with dots representing the partial differential with respect to time, and L_1 is a self-adjoint linear operator. Similar to discrete systems, a coordinate transformation $u = m^{1/2}(x) y$ will make above equation have the form

$$\ddot{u} + m^{-1/2}(x) L_1 m^{-1/2}(x) u = 0$$

or simply

$$\ddot{u} + L_2 u = 0$$

Here L_2 is self-adjoint. The modes $\phi_i(x)$ obtained from above equation can be normalized such that

$$\int_{0}^{L} \phi_{i}(x) \phi_{j}(x) dx = \delta_{ij}$$

The displacement u(x,t) of the beam is sampled at M locations, which give us a set of displacements as $u(t) = [u(x_1,t) \dots u(x_M,t)]^T$. This displacement is approximated as a truncated series of the linear normal modes

$$u(x,t) \approx \sum_{i=1}^{M} q_i(t) \phi_i(x) = \Phi^{T} \mathbf{q}$$

where $\phi = [\phi_1(x) \dots \phi_M(x)]^T$ is a vector of modal functions and $\mathbf{q}(t) = [q_1(t) \dots q_M(t)]^T$ is the vector of modal coordinates. Let us define a matrix

$$\Phi = [v_1 ... v_M]$$

where the vector $v_i = [\phi_i(x_1) \dots \phi_i(x_M)]^T$. Then we can write

$$\mathbf{u} = \Phi \mathbf{q}(\mathbf{t})$$

The above equation relates the discrete displacement of the beam to the discretization of the mode shapes $\phi_i(x)$. We can make an N×M ensemble matrix U by sampling displacements N times at M locations on the beam. This is written as

$$\mathbf{U} = [\mathbf{u}(t_1) ... \mathbf{u}(t_N)]^T = [\mathbf{\Phi}\mathbf{q}(t_1) ... \mathbf{\Phi}\mathbf{q}(t_N)]^T$$

or

$$\mathbf{U} = (\mathbf{\Phi} \ \mathbf{Q})^{\mathrm{T}}$$

where $\mathbf{Q} = [\mathbf{q}(t_1) \dots \mathbf{q}(t_N)]$ is an M×N matrix. Now we can make a correlation matrix as

$$\mathbf{R} = \frac{1}{N} \mathbf{U}^{\mathsf{T}} \mathbf{U} = \frac{1}{N} \Phi \mathbf{Q} \mathbf{Q}^{\mathsf{T}} \Phi^{\mathsf{T}}$$

To check that whether ν_j is an eigenvector of \boldsymbol{R} , post multiplying ν_j into \boldsymbol{R} as

$$\mathbf{R} \, \mathbf{v}_{j} = \frac{1}{N} \mathbf{\Phi} \, \mathbf{Q} \mathbf{Q}^{\mathsf{T}} \, \mathbf{\Phi}^{\mathsf{T}} \, \mathbf{v}_{j} \tag{2}$$

In the above equation $\Phi^T \nu_j$ has elements of the form ${\nu_i}^T \nu_j$. We assume that the spatial discretization is evenly spaced. Then we can say, using the rectangular rule, that

$$V_i^T V_j = \sum_{k=1}^M \phi_i(x_k) \ \phi_j(x_k) \approx \left(\frac{1}{h}\right) \int_0^L \phi_i(x) \ \phi_j(x) \ dx$$
(3)

where h is the spacing of the spatial discretization. Here we make an approximation as $\nu_i^T\nu_j\approx (1/h)\;\delta_{ij}\;.\;\text{The equation becomes}\;\Phi^T\nu_j\approx [0\;\ldots\;,0,1/h,0,\;\ldots\;0]^T=h_j\;.\;\text{With this result equation (2) takes the form}$

$$\mathbf{R} \, \mathbf{v}_{j} \approx \frac{1}{\mathbf{N}} \, \mathbf{\Phi} \, \mathbf{Q} \mathbf{Q}^{\mathsf{T}} \, \mathbf{h}_{j}$$

The *ij*th elements of \mathbf{QQ}^{T} are $\sum_{k=1}^{N} q_i(t_k) q_j(t_k)$

If the frequency of oscillation of q_i (t) and q_j (t) are incommensurate, then for a large number of samples

$$\lim_{N \to \infty} \frac{1}{N} \sum_{k=1}^{N} q_i(t_k) \ q_j(t_k) = 0 \qquad i \neq j$$

Thus

$$\lim N \to \infty \frac{1}{N} \mathbf{Q} \mathbf{Q}^{\mathrm{T}} = \mathbf{D}$$

Which is diagonal with diagonal elements

$$d_{ii} = \frac{1}{N} \sum_{k=1}^{N} q_i(t_k)^2$$

Which are mean squared values of $q_i(t)$.

In such case, $\mathbf{R}\mathbf{v}_j \to \mathbf{\Phi}\mathbf{D}\mathbf{h}_j \approx \mathbf{\Phi}\mathbf{h}_j \, \mathbf{d}_{jj} \approx \mathbf{v}_j \, \mathbf{d}_{jj}$ /h. So for large N with evenly spaced data when the modal frequencies are distinct, the discretized modal vectors \mathbf{v}_j approximately satisfy the eigenvalue problem associated with \mathbf{R} . In such case, it may be reasonable to expect that the POMs converge to \mathbf{v}_j , the discretized normal modes, and POVs converge to \mathbf{d}_{jj} /h, which is proportional to mean squared modal coordinates. This formulation has been tested numerically applying to the free vibration of a cantilever beam and a hinged-hinged beam. However, an experimental test has not been performed to verify this numerical simulation.

The crux of the approximate convergence of the POMs to discretized modes is in equation 3. In the approximate equality between the integral representing orthogonality of modes and the sum via the rectangular rule of integration. Immediately, we can suggest that results should increase in quality as the resolution of the discretization become finer.

2.4 Conventional Modal Analysis [4]

We have already discussed some conventional experimental techniques for modal frequencies and damping ratios. Determining the mode shapes from experimentally measured transfer functions is slightly more complicated and involves the measurement of several transfer functions. For a multi-degree-of-freedom system with harmonic input $(f \ e^{j\omega_d t})$, the response (**u**) is given by

$$u = (K - \omega_d^2 M + j\omega_d C)^{-1} f$$

where K, M and C are stiffness, mass and damping matrices respectively. A receptance matrix can be obtained as

$$\alpha(\omega_d) = \left(K - \omega_d^2 M + j\omega_d C\right)^{-1}$$

Assuming the damping to be modal, we can represent the matrices in diagonal form as

$$\Lambda_k = diag\left[\omega_i^2\right] = P^T M^{1/2} K M^{-1/2} P$$

$$\Lambda_c = diag[2\zeta_i\omega_i] = P^T M^{1/2} C M^{-1/2} P$$

where P is the normalized eigenvectors of the matrix $M^{-1/2}KM^{-1/2}$ and $P^{T}P = I$.

The receptance matrix can be written as

$$\alpha(\omega_d) = \left[S \operatorname{diag} \left[\omega_i^2 - \omega_d^2 + 2\zeta_i \omega_i \omega_d \right] S^T \right]^{-1}$$

where $S = M^{1/2}P$. The columns of S^{-T} are the mode shape vectors (\mathbf{u}_i) of an undamped system. Then the above equation can be written as

$$\alpha(\omega_d) = \sum_{i=1}^n \left[\frac{u_i \ u_i^T}{(\omega_i^2 - \omega_d^2) + (2\zeta_i \omega_i \omega_d)j} \right]$$
(1)

This equation provides a relation between receptance matrix and system's mode shapes.

The elements of the receptance matrix located at the intersection of sth row and rth column of $\alpha(\omega_d)$ is essentially the transfer function between the response at the point s and \mathbf{u}_s the input at the point r, \mathbf{f}_r , when all other inputs are held to zero. The srth element of $\alpha(\omega_d)$ is

$$\alpha_{sr}(\omega_d) = \sum_{i=1}^n \left[\frac{\left[u_i \ u_i^T \right]_{sr}}{\left(\omega_i^2 - \omega_d^2 \right) + \left(2\zeta_i \omega_i \omega_d \right) j} \right]$$

Since $\alpha(\omega_d)$ is a matrix, it can not be written as ratio of an output to an input. However each element can be written as transfer functions

$$\frac{u_s}{f} = [\alpha(\omega_d)]_{sr} = H_{sr}(\omega_d)$$

where $H_{sr}(\omega_d)$ is the transfer function between an input at point r and an output at point s. For the case $\omega_i = \omega_d$ equation (1) becomes

$$\left|u_i u_i^{\tau}\right| = \left|2\zeta_i \omega_r^2\right| \left|H_{sr}(\omega_i)\right|$$

The above equation gives magnitude of one element of matrix [$\mathbf{u_i} \mathbf{u_i}^T$]. The phase plot of $H\left(\omega_i\right)$ is used to determine the sign of the element. So in order to compute mode shapes, the knowledge of amplitude and phase at various locations is vital. In our case, due to floppy behavior of beam, this method is not applicable, as we cannot obtain the frequency response from an impulse excitation at all the desired locations, since the impulse is very small and does not trigger the signal analyzer. This shows the importance of the need of another method which can handle such situations.

While information is needed about the input for a conventional modal analysis, it is applicable regardless of knowledge of the mass distribution. Furthermore, it does not involve a rectangular-rule integration approximation, which is at the crux of the application of POD to continuous systems. Finally, traditional modal analysis can tie the identified mode-shapes to their modal frequencies while POD is geared to find mode shapes independently.

Chapter 3

Experimental Setup

We choose a cantilever beam because it is a well understood system which is easily sensed with strain gages. Another reason is that it is relatively inexpensive and easy to build. In this chapter a discussion about the experimental setup and the interface between different hardware elements is presented. We will also see the conversion of voltage signal generated by the strain gage conditioner to strain and then to displacement. Some physical properties like modal frequencies and damping factors for the beam are computed theoretically and experimentally in this section. First we review the theoretical model of a cantilever beam.

3.1 Beam Model

We are considering a well understood system, so that we can compare the results with POD process. For this theoretical model, we assume that the beam used has uniform cross sectional area. It is homogenous, isotropic and obeys Hook's law within the elastic limit. We also assume uniform mass distribution and elasticity in the beam and ignoring

rotational inertia. Cross sections perpendicular to neutral axis remain planar or there is no shearing is occurring in the beam. A unforced model of a cantilever is

$$m(x)\ddot{y} + L_1 y = 0$$

where y(x,t) is the displacement, with dots representing the partial differential with respect to time, and $L_1 = E I y_{xxxx}$ is a self-adjoint linear operator with y_{xxxx} as the fourth derivative with respect to x. E and I are the Young's modulus and area moment of inertia of the system. The boundary conditions for this system are

$$y(0,t) = 0$$
 Zero displacement at the fixed end $y_x(0,t) = 0$ Zero slope at the fixed end $y_{xx}(\ell,t) = 0$ Zero moment at the free end $y_{xxx}(\ell,t) = 0$ Zero shear at the free end

where ℓ is the total length of the beam.

3.2 Physical Beam

The main parameter needed for the application of proper orthogonal decomposition is the displacement or velocity information at different locations. The displacements of the beam at various locations can be taken by using proximity probes, laser transducers, strain gages or accelerometers. We choose to use strain gages because they have minimal effect on the dynamics, and have good behavior in the frequency range of our experiment. Other reasons were the low cost of strain gages and the availability of strain gage conditioners in the lab.

The cantilever is consists of a 0.3937 \times 0.012 \times 0.00079 m³ beam of mild steel with one end fixed in a steel clamp. The beam has Young's modulus $E = 128 \times 10^9 \text{ N/m}^2$ and a density $\rho = 7488 \text{ kg/m}^3$. The coordinates for this system are taken as x along the length, y along the thickness and z along the width of the beam. The displacements at various points are measured with the help of strain gages. Twelve strain gages were used to make six half wheat-stone bridges.

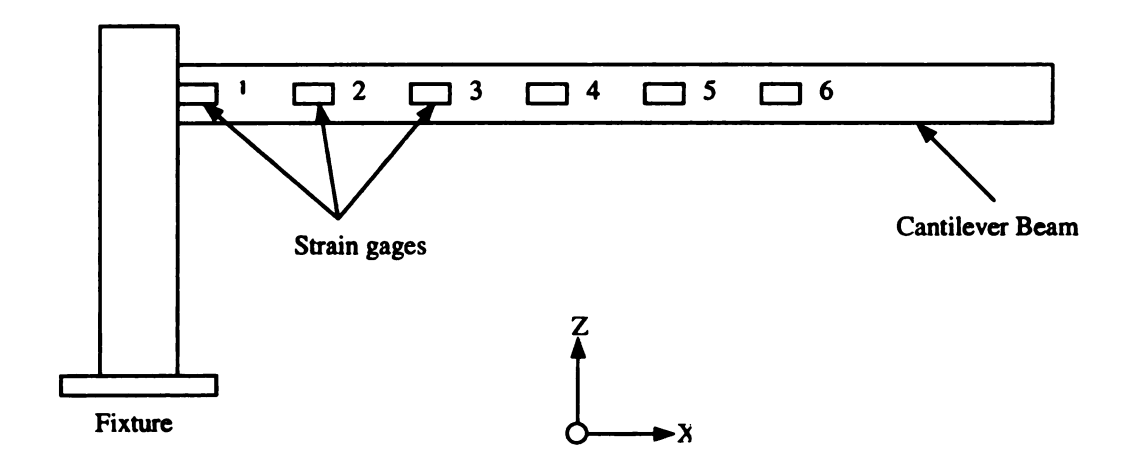


Figure 3.1: Cantilever beam with strain gages. The beam displacement is normal to the page.

The strain gages were mounted starting from fixed end to the free end at equal distances and numbered them form 1 to 6, starting from fixed end as shown in Figure 3.1. The gages were spaced equally at 0.049 m. We did not put more than six strain gage circuits due to the finite length of the beam. Another important factor was the concentration of strain towards the fixed end, and minimal strain at free end. For this reason, the gage locations are biased towards the clamped end to improve sensitivity. The

locations were "optimized" by performing numerical simulations and iterating the gage locations [5]. However, a rigorous optimization procedure has not been performed.

3.3 Strain gages and instrumentation

All the strain gages are of the type Micro-Measurements Precision Strain Gage model CEA-06-250UN-350. These have resistance of 350 ± 0.3 %, a gage factor of 2.1 ± 0.5 % and transverse sensitivity of $(+0.1\pm0.2)$ % all at 24 °C. For minimizing the effect of wiring, we used Micro-Measurements single conductor wire type 134-AWP. To reduce the effect of noise, we twisted the three wires coming out of each strain gage pair, representing half bridge.

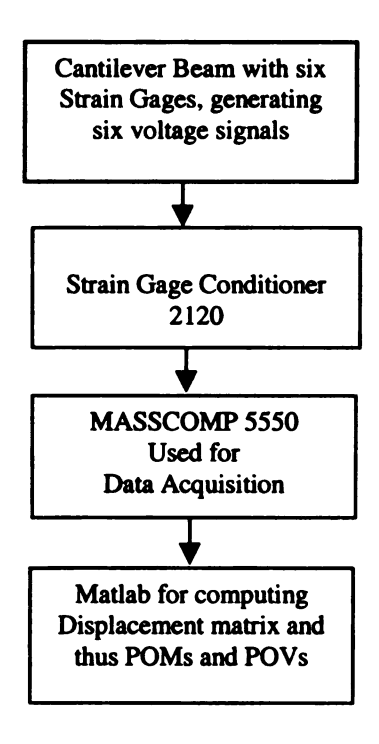


Figure 3.2: Block diagram showing data acquisition process

The voltage signal from strain gages was conditioned in strain gage conditioners model 2120 from Micro-Measurements Group Inc. A gain of 2000 was used on the strain gage conditioner and an excitation voltage of 10V was used to excite the circuit. Each half bridge was balanced prior to collecting the data. For data acquisition we used Laboratory Workbench of Concurrent Computer Corporation on a MASSCOMP 5550. Various sampling rates up to 1000 samples/seconds were used for data acquisition. The limit on the sampling rate was due to the memory available on MASSCOMP. The data was taken with different time record lengths and with varying number of samples to see the effect on accuracy of results.

3.4 Voltage to strain

An electrical-resistance strain gage will change in resistance due to applied strain according to the equation

$$\frac{\Delta R}{R} = S_s \varepsilon \tag{1}$$

where $\Delta R/R$ is the change in resistance per original resistance, S_g is the gage factor, and ϵ is the strain. The gage factor and resistance parameters are generally provided by the manufacturer. As we are using half wheat-stone bridges for strain measurement, we will have two active resistances in the circuit as shown in Figure 3.3. Then for the change in voltage E across the circuit we have

$$\Delta E = V \frac{R_1 R_2}{(R_1 + R_2)^2} \left(\frac{\Delta R_1}{R_1} - \frac{\Delta R_2}{R_2} \right)$$
 (2)

where V is the excitation voltage and R_1 and R_2 are the resistances of two strain gages in the half bridge circuit.

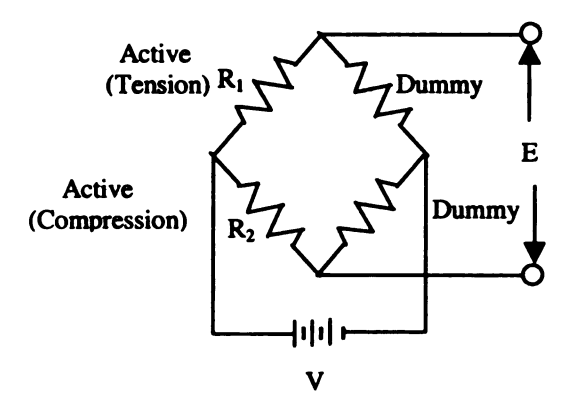


Figure 3.3: Resistances forming "half wheat-stone bridge circuit" configured for bending.

As all the strain gages have the same gage factor, and if the strain on one is due to compression then the strain on the other will be due to tension or $\varepsilon = \varepsilon_1 = -\varepsilon_2$, then eq. 2 using eq.1 gives

$$\mathcal{E} = \frac{\Delta E}{V} \frac{(R_1 + R_2)^2}{R_1 R_2} \frac{1}{2S_*}$$
 (3)

After plugging in the known parameters values in eq. 3 we obtained a conversion factor for voltage to strain, using gain factor of 2000, as

$$\varepsilon = \Delta E \times 2000 \times 0.095238095 = \Delta E \times 190.4762$$

The gain factor was used to amplify the voltage signals from strain gage conditioners as they were very weak.

3.5 Strain to displacement

The strain $\varepsilon(x)$ in a symmetric beam subjected to bending is related to the transverse displacement y(x) by

$$\varepsilon_{xx} = c \frac{\partial^2 y}{\partial x^2}$$

where c is half the width of beam. By approximating

$$y(x,t) = \sum_{i=1}^{n} \phi_i(x) u_i(t)$$

where $\phi_i(x)$ form a basis satisfying the geometric conditions, we can write the strain as

$$\varepsilon_{xx}(x) = c[\psi_1(x)....\psi_n(x)]\begin{bmatrix} u_1(t) \\ \vdots \\ u_n(t) \end{bmatrix}$$

where

$$\psi_i(x) = \frac{\partial^2 \phi_i(x)}{\partial x^2}$$

Now taking strains at n different points of the beam, we can have n such equations which can be written in matrix form as

$$\begin{bmatrix} \mathcal{E}_1 \\ \vdots \\ \dot{\mathcal{E}}_n \end{bmatrix} = c \begin{bmatrix} \psi_{11} \dots \psi_{1n} \\ \vdots \\ \psi_{n1} \dots \psi_{nn} \end{bmatrix} \begin{bmatrix} u_1 \\ \vdots \\ u_n \end{bmatrix}$$

or $\epsilon = c \Psi u$

where $\Psi_{ii} = \psi_i(x_i)$

 $u=[u_1,...,u_n]^T$, $\varepsilon=[\varepsilon_1,...,\varepsilon_n]^T$ and ε_i indicate the strain measured at the ith location x_i . If we express the displacements y(x,t) at locations x_k with similar notation, we write

$$\begin{bmatrix} y_1 \\ \vdots \\ y_p \end{bmatrix} = \begin{bmatrix} \phi_{11} \cdot \cdot \cdot \cdot \phi_{1n} \\ \cdot \cdot & \cdot \\ \vdots \\ \phi_{p1} \cdot \cdot \cdot \cdot \phi_{pn} \end{bmatrix} \begin{bmatrix} u_1 \\ \vdots \\ u_n \end{bmatrix}$$

or
$$y = \Phi t$$

where $\phi_i(x_j)$ form a basis satisfying the geometric boundary conditions. Assuming ψ is invertible, we can solve for y in terms of ε , such that

$$\begin{bmatrix} y_1 \\ \vdots \\ y_p \end{bmatrix} = \frac{1}{c} \begin{bmatrix} \phi_{11} \dots \phi_{1n} \\ \vdots \\ \phi_{p1} \dots \phi_{pn} \end{bmatrix} \begin{bmatrix} \psi_{11} \dots \psi_{1n} \\ \vdots \\ \vdots \\ \psi_{n1} \dots \psi_{nn} \end{bmatrix}^{-1} \begin{bmatrix} \varepsilon_1 \\ \vdots \\ \varepsilon_n \end{bmatrix}$$

Note that while y(x,t) can be evaluated at any x_k , k=1,2,...,p, there can only be n independent displacements. Later, we try using p>n to see if extra "pseudo sensors" might provide a means of interpolation of data.

3.6 Identification of modal frequencies and damping ratios.

Theoretical modal frequencies from model in section 3.1 were computed using

$$\omega_n = \beta_n^2 \sqrt{\frac{EI}{A\rho}}$$

where β_n are the weighted frequencies per unit length, and $I=bh^3/12$ is the area moment of inertia with b as the width and h being the thickness of the beam. A is the cross sectional area of the beam and ρ is the volumetric density of the beam material.

With values of " β_n ?" from Inman [4] (where ? is the length of the beam) for first six modes as 1.87510407, 4.69409113, 7.85475744, 10.99554073, 14.13716839, 17.278759, we obtained the theoretical modal frequencies as 4.52, 28.36, 79.38, 155.57, 257.17, 384.17Hz.

For experimental modal testing, it is hard to decide the effective number of degrees of freedom. One way is to count the clearly defined number of peaks or resonances, which can be bad if the structure has closely spaced natural frequencies. A good method to use is called single-degree-of-freedom curve fit. In this method the compliance is sectioned off into frequency ranges breaking each successive peak. Each peak is then analyzed by assuming that it is the response of a single-degree-of-freedom system. An assumption in this is that in the vicinity of the resonance, the frequency response function is dominated by that single mode [4]. We used this method to find the natural frequencies and modal damping ratios of the system.

In our experiment we used the A&D Co. Ltd.'s AD 3525FFT Analyzer to graphically see the frequencies present in the signal. We used impulse hammer to give an input to the system and recorded the FFT response on the analyzer. In order to increase accuracy we took an average of ten inputs. The experimental values are 4.5, 27.25, 75.5, 147.5, 243.75, 365 Hz. The error with the theoretical frequencies obtained from model in section 3.1, was 0.44, 3.91, 4.88, 5.18, 5.21, and 4.98 percent respectively. Theoretical frequencies are higher than the experimental ones. The theoretical frequencies come from a model which involve assumptions. Assumptions are effectively associated with

constraints, which typically stiffen a system and increase the natural frequencies. The error in results also depends upon how accurately the data is acquired. Presence of noise in the signal, improper interface of hardware elements, quality of software and hardware used and human error can be counted towards the error cause. A graphical comparison is present in figure 3.4.

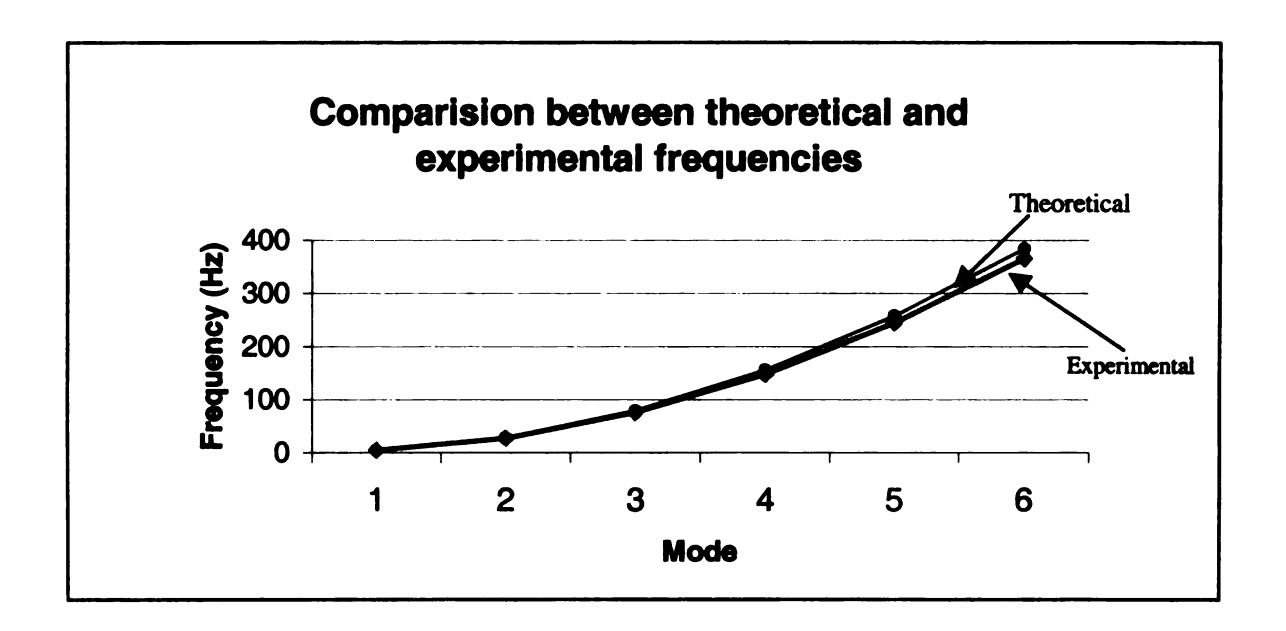


Figure 3.4: Comparison between theoretical and experimental frequencies of cantilever beam.

The damping ratio associated with each peak is assumed to be the corresponding modal damping ratio ς_i , in the modal coordinate system. Each peak was considered separately. For a system with light enough damping, so that the peak is well defined, the modal damping ς is related to the frequency corresponding to the two half power points as shown in figure 3.5.

$$|H(\omega_a)| = |H(\omega_b)| = \frac{|H(\omega_d)|}{\sqrt{2}}$$

With $\omega_a - \omega_b = 2\varsigma \omega_d$ we found damping ratios ς as

$$\varsigma = \frac{\omega_b - \omega_a}{2\omega_d}$$

where ω_d is the damped natural frequency of the system. We obtained the values of ω_a , ω_b , and ω_d using the plots on the FFT analyzer. It was easy for us to read the values on the analyzer as we can snap to the peaks with the cursor and read the exact values of frequency related the peaks or half-power points. We assumed the peak frequency of damped system equal to damped natural frequency of the system as the system was lightly damped.

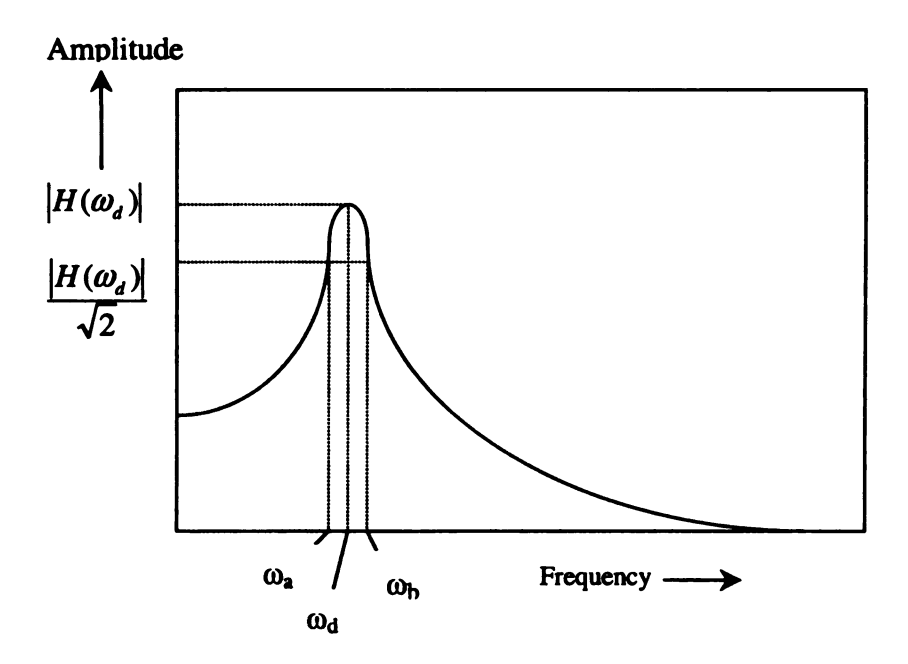


Figure 3.5: Illustration of the calculations of damping ratios by using quadrature peak picking method for lightly damped systems

We found the damping ratios as 0.01606, 0.0158, 0.009, 0.00467, 0.0031, and 0.00224. The accuracy of damping ratios depends upon the frequency resolution and how preciously the plots were read for the values of half power points. We tried to find the mode shapes with a method discussed by Inman [4]. In that method we need to measure impulses at several locations of the beam to produce frequency response associated with inputs at those locations. Our beam was so floppy that we were unable to generate meaningful signal on the impulse hammer. This points to an advantage of the POD method, for which multiple input locations are not generally needed. This method can be applied for a fixed fixed beam, which can be helpful for comparison with POMs.

We also computed time constant ($1/\varsigma\omega_n$) and settling time (2% settling time is close to $4/\varsigma\omega_n$) for each mode which are tabulated in Table 3.1.

Mode	Time Constant	Settling Time
	Experimental	Experimental (sec)
1	13.837	55.348
2	2.3226	9.2904
3	1.4716	5.8866
4	1.4517	5.8069
5	1.3234	5.2936
6	1.2230	4.8923

Table 3.1: Experimental values of time constant and settling time for each mode.

Node points for each mode is provided in Table 3.2. These points are obtained by plotting linear normal modes.

Modes	Node Positions, in x
1	No node
2	0.3084 m
3	0.1982 m
	0.3413 m
	0.1411 m
4	0.2531 m
	0.3656 m
	0.1097 m
5	0.1968 m
	0.2843 m
	0.3718 m
	0.0899 m
	0.1611 m
6	0.2326m
	0.3042m
	0.3758 m
6	0.0899 m 0.1611 m 0.2326m 0.3042m

Table 3.2: List of node points for the first six linear normal modes of a cantilever beam, measured in x from the fixed end.

Chapter 4

Tests and Results

In this chapter we discuss different tests performed and their results. We have divided the tests in four sections. In first section, the effect of the sampling rate on the accuracy of POMs is studied. The second section discusses the behavior of POMs with varying sample lengths, in third attempt we applied input at different points of beam to see behavior of POMs. In order to improve the resolution of our results, we applied an idea of putting "pseudo sensors" between our real sensors. To check the validity of this process two sets of admissible functions were made and used as basis functions. We also applied the idea of pseudo sensors to both these set of functions. Lastly we try to extract modes directly from strains. Actually this is to study the feasibility of applying POD at various stages of data analysis. The results are compared with the linear normal modes (LNMs) of vibration and the data for these normal modes was taken from the book Engineering Vibration by D. J. Inman [4]. An impulse input was given to the beam to excite the modes.

4.1 POD with various sampling rates

The selection of an impulse input for the system was due to the reason that it can excite maximum number of frequencies possessed by the system. Although it is not easy to give an ideal impulse, it still works. Our first experiment was to acquire data at different sampling rates and various time records. The software has the capability of acquiring data up to 5000 samples per second. But with higher sampling rates the size of data files will increase, and the unavailability of memory, restricted us to work under 1000 samples per second. We used four different sampling rates i.e. 1000, 800, 400 and 100 samples per second to compare the accuracy of the results. The modal frequencies computed in section 3.5 range from 4 to 384 Hz. So for the case of sampling rates of 100 and 400, the high frequencies will be aliased.

The POMs were normalized for the sake of comparison. Both POMs and LNMs are plotted on the same graphs to compare both modes. We have formulated our plots to give us the mode shapes of the cantilever and not the displacement of the point where the strain gages are located. So plots are of displacements that are located on the beam equally spaced along the whole length. The first point for the plots is taken as zero as there is zero displacement at the fixed end. For easy comparison, norm of the error for each mode was calculated and presented with each test. For this we normalized both the POMs and LNMs and found the difference between them. The norm of error provides us with the information that how much content of each mode is present in a particular mode shape, while POVs tell us about the energy contents of each mode.

For the first attempt we tried a sampling rate of 100 samples per second with 250 samples. A time record of 2.5 seconds is enough for capturing characteristics of the signal as during this time none of the mode died down. Settling time for each mode can be seen in Table 3.1. As the beam was given input at the free end, the first couple of modes were more likely to be excited. Figure 4.1 with Table 4.1 shows the POMs, their corresponding POVs and the norm of error computed for each mode. The continuous line shows the linear normal modes and the circles show the POMs. With a sampling rate of 100 samples/second, we can see that POMs are converging to linear normal modes. As the input was at the free end, so chances are more of excitation of 1st mode. The POVs also indicate the maximum amount of energy in the first mode.

When the sampling rate is increased to 400 samples/second with 250 samples, some encouraging results can be seen. Figure 4.2 and Table 4.2 gives the details about POMs and POVs. Here a change in the numeric values can be seen, we can say that the results are more accurate as compared to the previous results due to high sampling rate. First mode is similar to the natural modes for a cantilever beam. The rest of the modes are close, but a little deviated. By looking at the eigenvalues or POVs, we come to know that first two modes have the highest energy or power and the rest of the modes have less energy. This may be partly due to the location of the excitation at the end of the beam.

With sampling rate of 800, we used a large number of samples. For this case the number of samples used were 4000. The data was acquired for five seconds. By looking at the settling time in Table 3.1, we can see that in 5 second time all the information for that last five modes is available. So we can say that this is a good selection of sampling rate and time window to capture the characteristics of the signal. A bit more accurate results are expected which can be seen in Figure 4.3 and table 4.3. Here the results are a little different, and we can see that first and last two modes are excited mostly. There is a change in the magnitude of POVs, but over all picture of the energy distribution in the modes is quite similar.

Figure 4.4 with Tables 4.4 provide the results when the sampling rate is 1000 samples/seconds with 4000 samples. Similar trend can be seen here. POVs are quite similar to the last results. Here first four modes are excited more. The excitation of a specific mode depends upon the initial conditions provided to the system and may be more number of strain gages. We were limited to this sampling rate due to memory constraint.

The conclusion of this section is that the computation of the lower modes is quite robust to the choice of the sampling frequency, even when the Nyquest Criterion is not met for all modes.

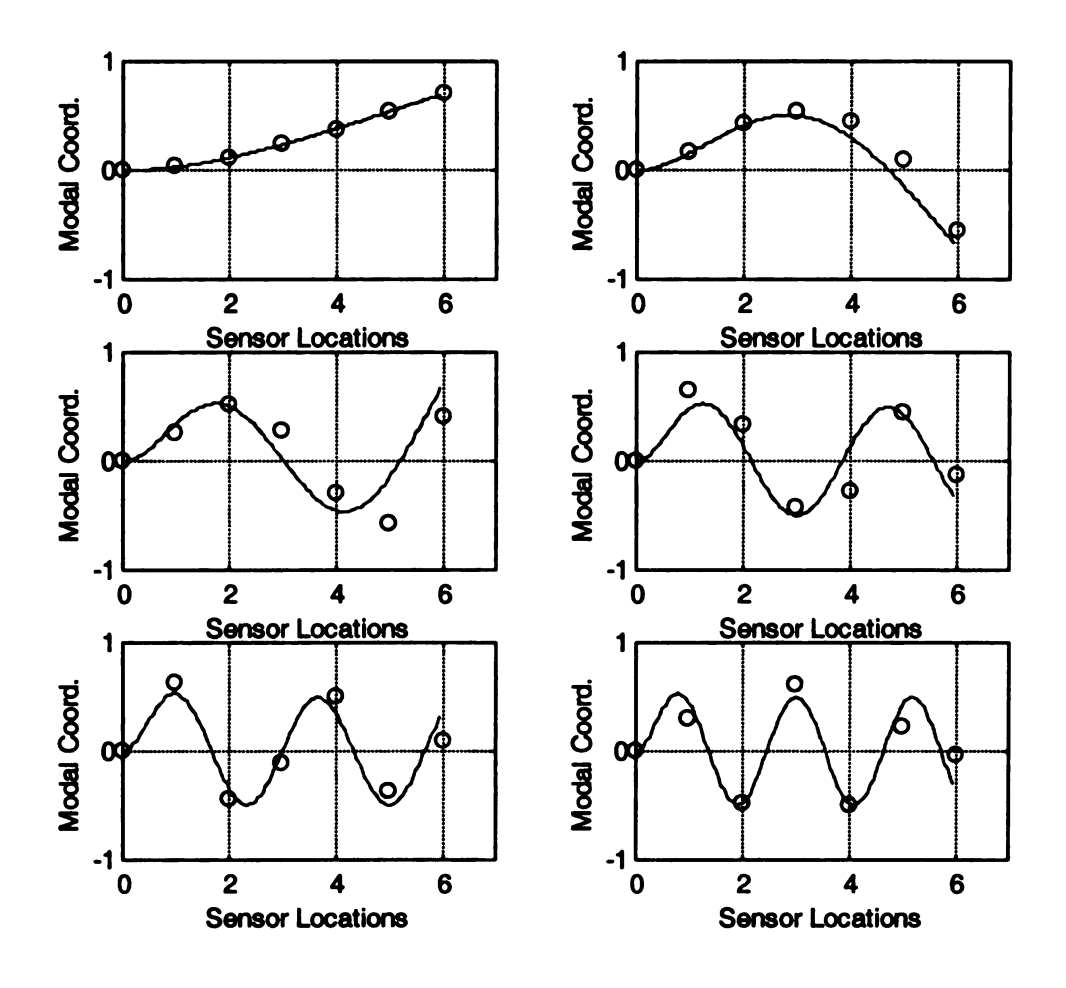


Figure 4.1: Proper orthogonal modes with sampling rate of 100 samples per second

POMs	$Norm = \ \phi_n - \nu\ $	POVs
1	0.0119	4.0145
2	0.3139	6.3503×10^{-4}
3	0.5914	5.9517× 10 ⁻⁵
4	0.5469	3.1631× 10 ⁻⁶
5	0.3843	1.0233× 10 ⁻⁷
6	0.3895	4.1540× 10 ⁻⁹

Table 4.1: Norm of error with LNMs for each mode and their corresponding proper orthogonal values for sampling rate of 100 samples per second.

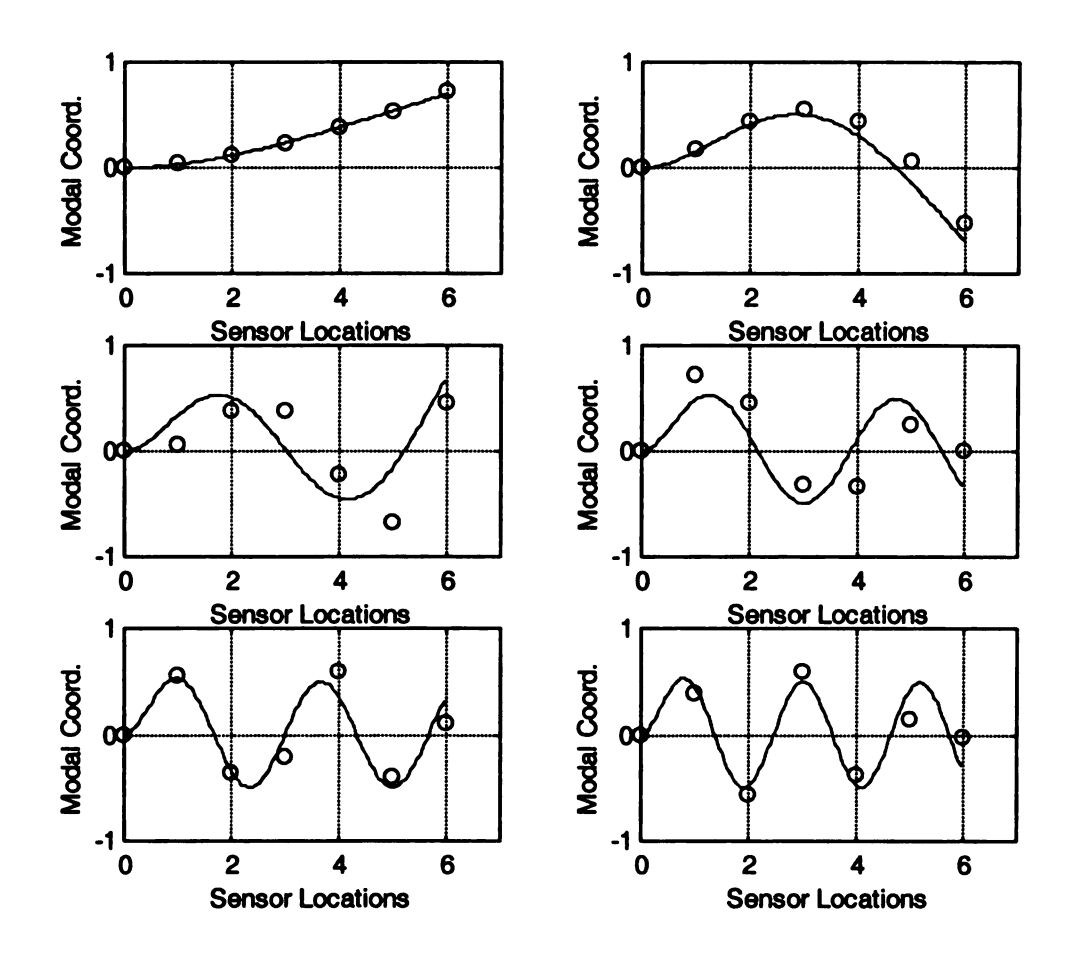


Figure 4.2: Proper orthogonal modes with sampling rate of 400 samples per second

POMs	$Norm = \ \phi_n - \nu\ $	POVs
1	0.0175	6.922
2	0.3053	1.332×10^{-3}
3	0.7721	2.267× 10 ⁻⁵
4	0.7882	2.864× 10 ⁻⁶
5	0.3858	4.785× 10 ⁻⁸
6	0.3996	3.221× 10 ⁻⁹

Table 4.2: Norm of error with LNMs for each mode and their corresponding proper orthogonal values for sampling rate of 400 samples per second.

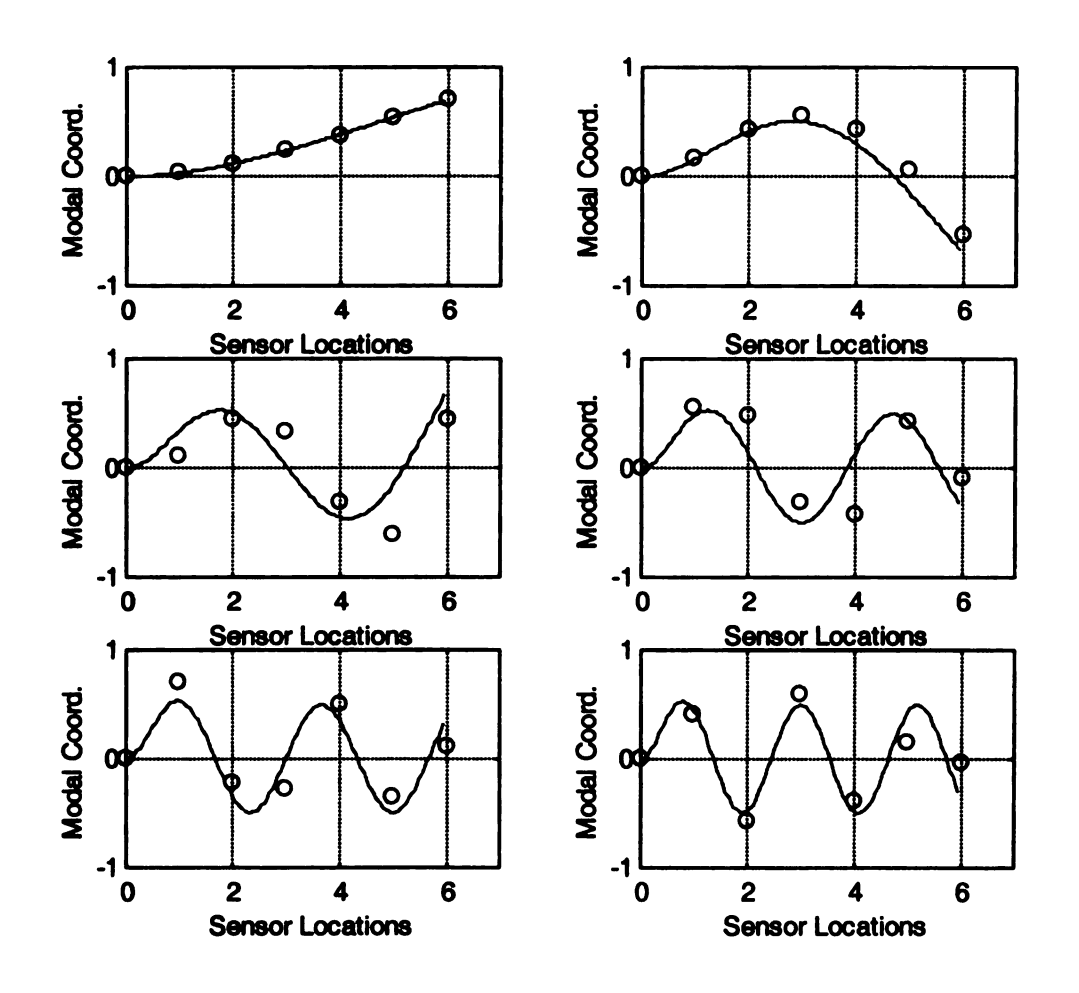


Figure 4.3: Proper orthogonal modes with sampling rate of 800 samples per second

POMs	$Norm = \ \phi_n - \nu\ $	POVs
1	0.0091	1.4585
2	0.2976	2.094× 10 ⁻⁴
3	1.8863	3.235× 10 ⁻⁶
4	1.8515	3.760× 10 ⁻⁷
5	0.4871	1.607× 10 ⁻⁸
6	0.4249	2.700× 10 ⁻⁹

Table 4.3: Norm of error with LNMs for each mode and their corresponding proper orthogonal values for sampling rate of 800 samples per second.

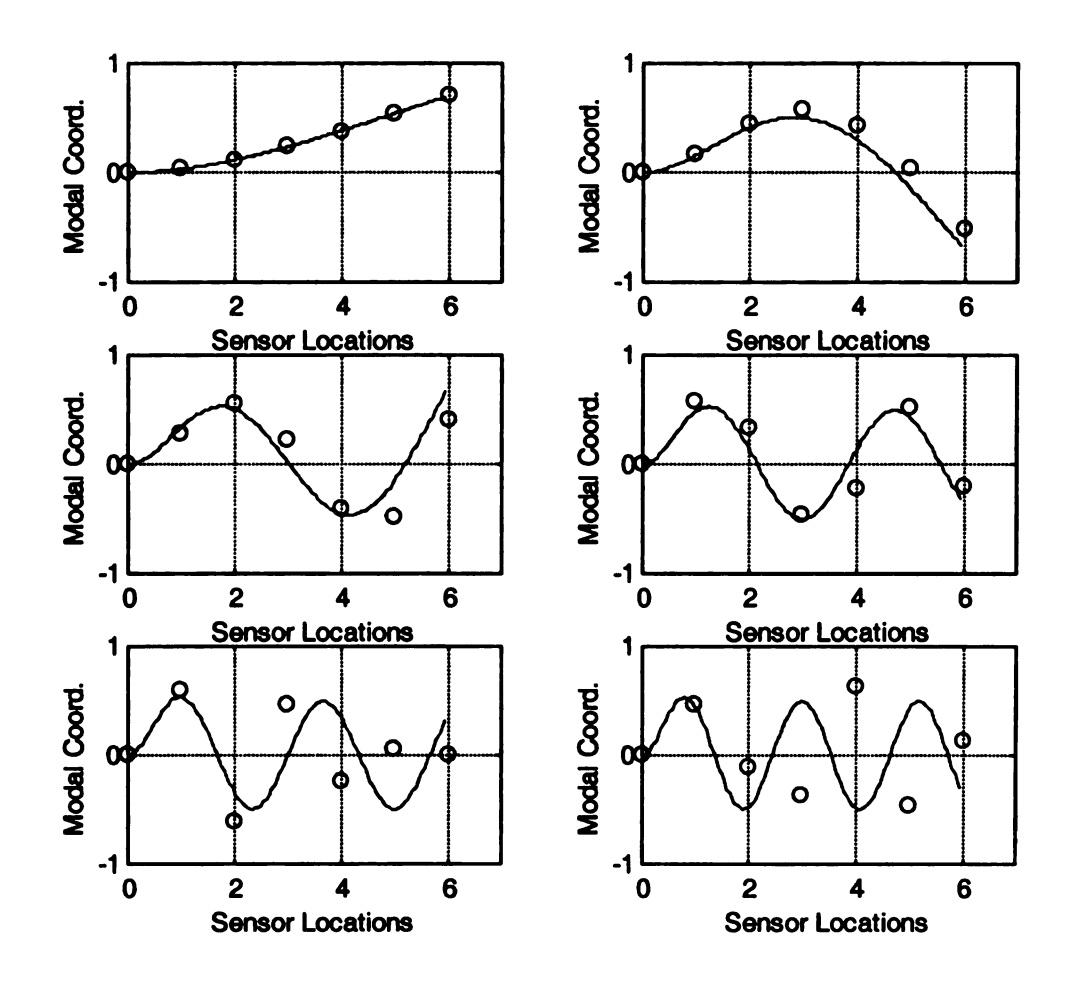


Figure 4.4: Proper orthogonal modes with sampling rate of 1000 samples per second

POMs	$\mathbf{Norm} = \left\ \phi_n - \nu \right\ $	POVs
1	0.0096	1.8315
2	0.2963	1.634× 10 ⁻³
3	0.4848	1.023× 10 ⁻⁵
4	0.4482	1.933× 10 ⁻⁶⁵
5	1.0566	8.158× 10 ⁻⁹
6	1.0705	1.318× 10 ⁻⁷

Table 4.4: Norm of error with LNMs for each mode and their corresponding proper orthogonal values for sampling rate of 1000 samples per second.

4.2 POD with input at various points of the system

In this section the effect of application of input at various points of the cantilever is studied, to see whether we can excite other modes better by providing different initial conditions. In previous section the system was excited by input at the free end. In the results we found that mostly first mode is excited, which motivated us to try input at different locations of the beam. In these experiments all the data is acquired at a sampling rate of 800 samples/second and for a time record length of one second.

For the first test, input was given between 4th and 5th strain gages which are located on beam at 0.15227m and 0.20127m from the fixed end. The details of the node points for different modes can be seen in Table 3.2. The numbering of strain gages starts from 1 to 6, where 1 is close to the fixed end. We plotted the POMs and LNMs on the same graphs to compare both results. The norm of error provides us with the information that how much content of each mode is present in a particular mode shape, while POVs tell us about the energy contents of each mode. Figure 4.5 and Table 4.5 indicate that nearly all the modes, contributes to this response. So we can see that impulse has excited all the modes, the reason of excitation of first mode more are the initial conditions.

When the input is given between 3rd and 4th strain gage, first four mode are excited the most, which can be seen in Figure 4.6 and Table 4.6. There are nodes present for 4th and 5th modes in the area of application of impulse. So we can say that force was applied at or close to a node point of 5th mode and a bit far from 4th mode node point, which allowed slight excitation of 4th mode. For the next test, input is given between 2nd

and 3rd strain gage. In this area a node points for 6th mode is present. Figure 4.7 and Table 4.7 give us the excitation of nearly all the modes except the 6th mode. Lastly when the input is applied between 1st and 2nd strain gage all the modes were excited as there is no node point for any mode near the area of application of force.

So we can observe that by giving various initial conditions to the system we can excite different modes especially the lower frequency modes. This could effect the efficacy of POD process. The little discrepancies in the results can be attributed towards the improper application of impulse or limitations of the data acquisition system. Here we can again say that this method is pretty robust for first 3 modes.

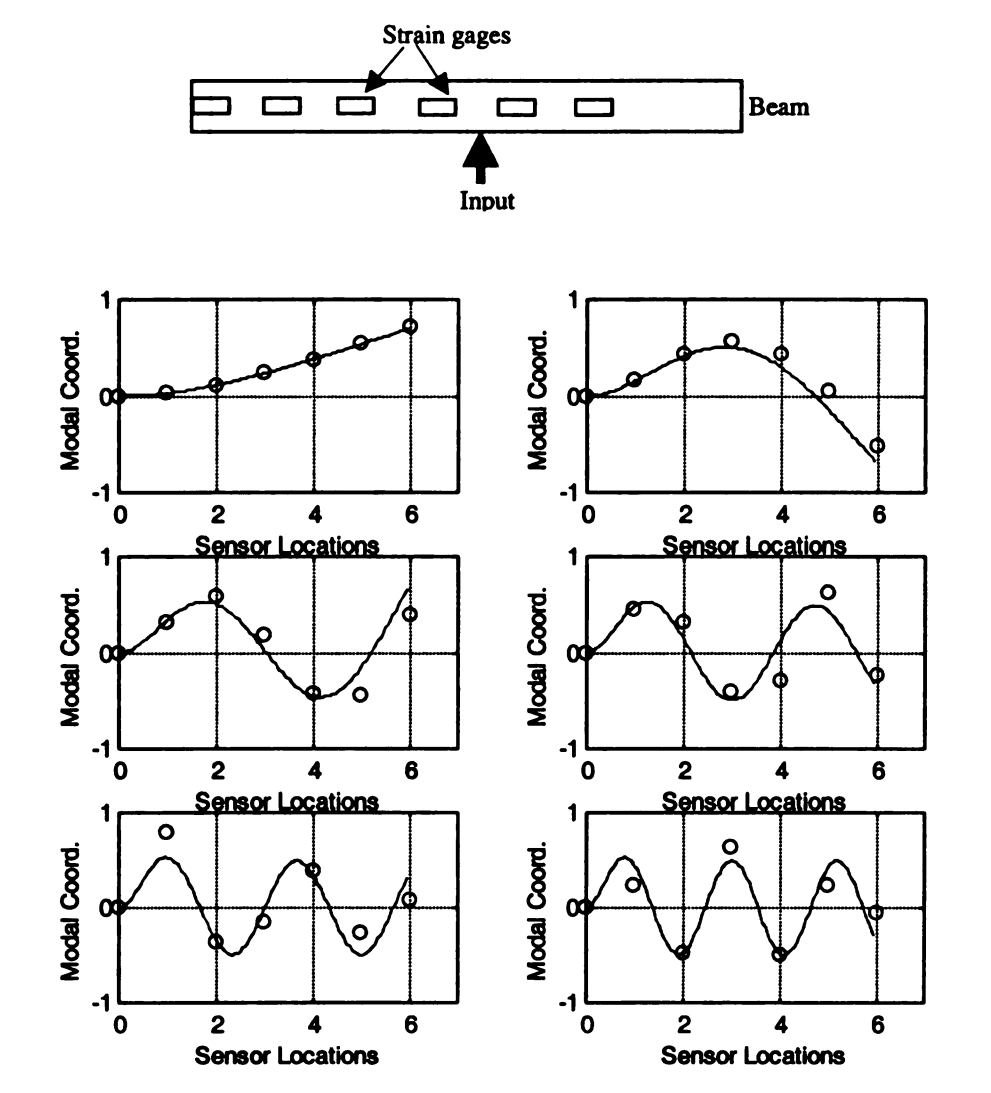


Figure 4.5: Proper orthogonal modes with sampling rate of 800 samples per second and force applied between 4th and 5th strain gage

POMs	$\mathbf{Norm} = \left\ \phi_n - \nu \right\ $	POVs
1	0.0101	2.8837
2	0.2974	3.7411× 10 ⁻³
3	0.4579	1.1931× 10 ⁻⁵
4	0.5277	1.1909× 10 ⁻⁶
5	0.4724	2.2223× 10 ⁻⁸
6	0.4068	1.5266× 10 ⁻⁹

Table 4.5: Norm of error with LNMs for each mode and their corresponding proper orthogonal values for sampling rate of 800 samples per second.

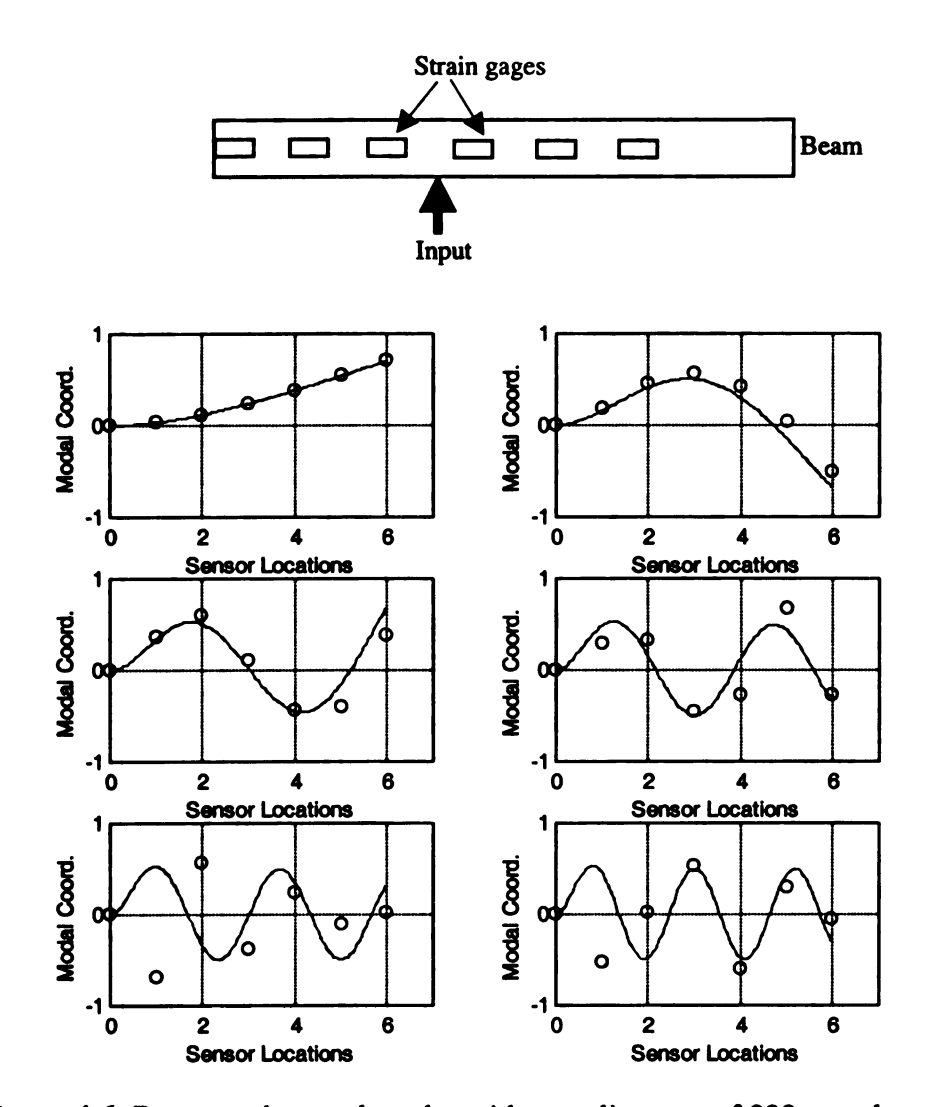


Figure 4.6: Proper orthogonal modes with sampling rate of 800 samples per second and force applied between 3rd and 4th strain gage.

POMs	$Norm = \ \phi_n - \nu\ $	POVs
1	0.0118	1.1682
2	0.2963	8.1544× 10 ⁻³
3	0.4155	5.0564× 10 ⁻⁵
4	0.5656	1.031×10 ⁻⁶
5	1.6968	8.2399× 10 ⁻⁹
6	1.0841	2.6738× 10 ⁻⁸

Table 4.6: Norm of error with LNMs for each mode and their corresponding proper orthogonal values for sampling rate of 800 samples per second.

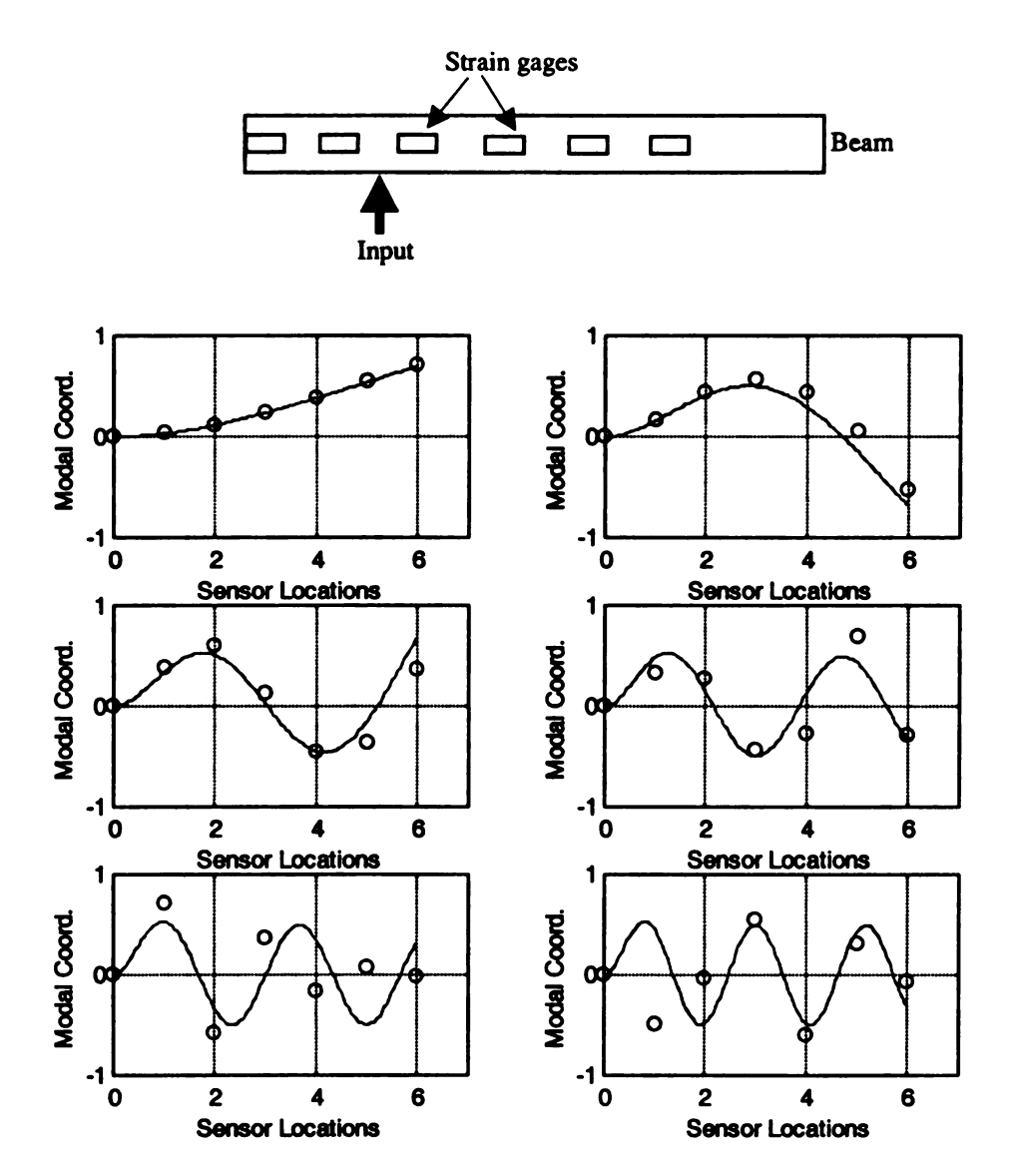


Figure 4.7: Proper orthogonal modes with sampling rate of 800 samples per second and force applied between 2nd and 3rd strain gage.

POMs	$Norm = \ \phi_n - \nu\ $	POVs
1	0.0106	1.0103
2	0.2986	3.4006× 10 ⁻³
3	0.4298	6.7788× 10 ⁻⁶
4	0.5482	3.5322× 10 ⁻⁷
5	0.9924	5.6277× 10 ⁻¹⁰
6	1.0281	3.6034× 10 ⁻⁹

Table 4.7: Norm of error with LNMs for each mode and their corresponding proper orthogonal values for sampling rate of 800 samples per second.

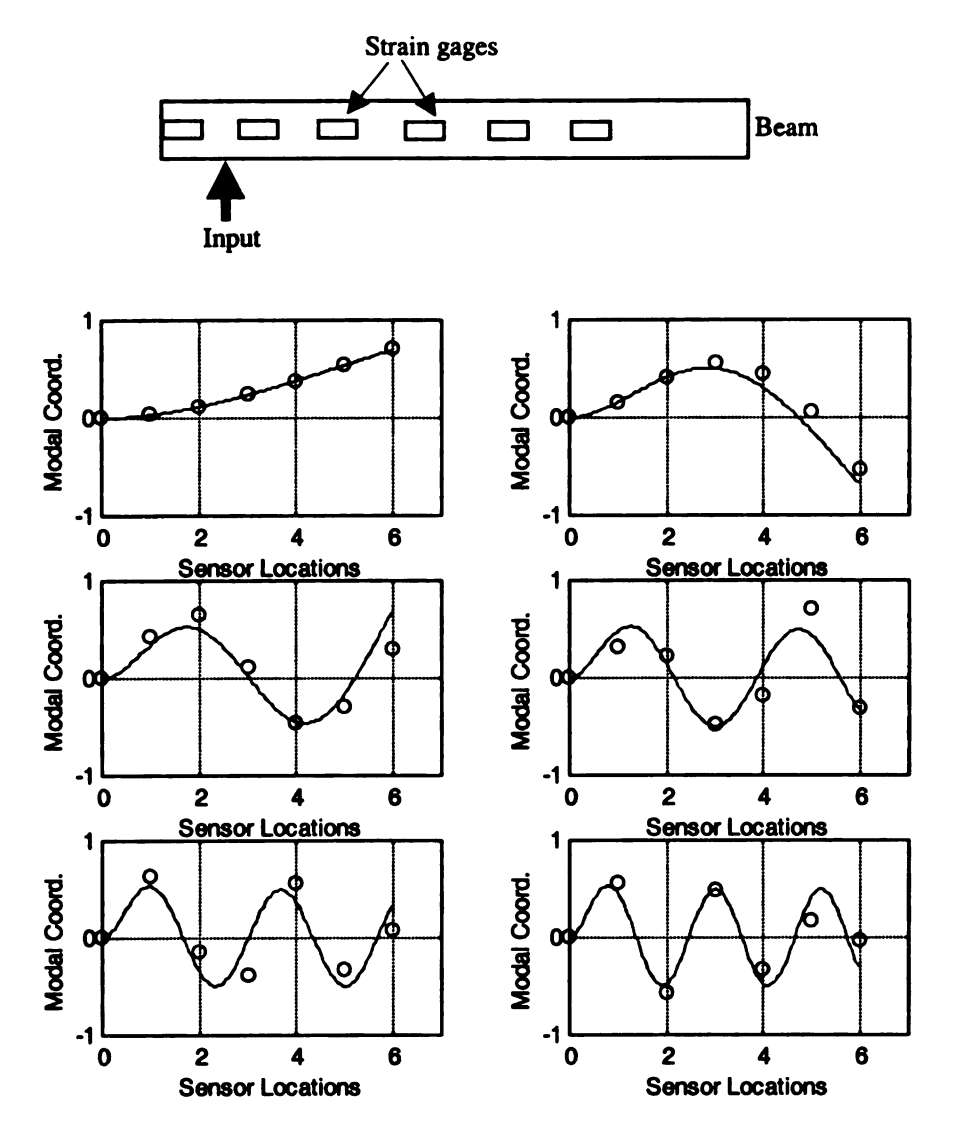


Figure 4.8: Proper orthogonal modes with sampling rate of 800 samples per second and force applied between 1st and 2nd strain gage.

POMs	$Norm = \ \phi_n - \nu\ $	POVs
1	0.0105	0.14704
2	0.3083	2.5044× 10 ⁻²
3	0.4585	2.5450× 10 ⁻³
4	0.4605	4.6211×10 ⁻⁵
5	0.5999	1.6238× 10 ⁻⁶
6	0.4232	7.8967× 10 ⁻⁸

Table 4.8: Norm of error with LNMs for each mode and their corresponding proper orthogonal values for sampling rate of 800 samples per second.

4.3 POD with variable time record length

In this section we will observe the effect of time record length on the validity of POD process. A sampling rate of 800 samples/second was used for all these experiments. The reason for selection of this sampling rate is the satisfaction of Nyquist criterion. The time record length used for tests are 0.0075, 0.025, 0.25, 0.5 and 1.0 seconds, which contain 6, 20, 200, 400 and 800 samples respectively, was used to observed the response of POMs. The justification for selection of such small time record lengths is that there are enough harmonics present to describe the characteristics of the signal. We used the data of the test, when the input was applied between 4th and 5th strain gage. We choose this impulse location since it led to one of the better results in section 4.2.

For first attempt, only 6 samples were used to observe the accuracy of the POMs. The results show that, even a small number of data, if taken at a high sampling rate, preserve the gist of the mode shapes. This can be seen in Figure 4.9 and Table 4.9. The magnitude of the POVs are small, the reason for this can be that POVs represent mean squared values. They therefore vary with the magnitude and location of impulse, and since we do not normalize with respect to the input, we expect variation in the magnitude of POVs anyway. Key things for obtaining modes are POMs and *relative* values of POVs. Here we can see the excitation of first four modes mostly. When we try with 20 samples, the results show excitation of nearly all six modes, as in Figure 4.10.

A time record length of 0.25 sec. showed a change in the results. A significant difference in POVs, shows the effect of time record length. Figure 4.11 and Table 4.11 shows the excitation of nearly all the modes. With 400 samples, the results are quite

similar to the pervious one. So we can see the results converging to certain values as number of samples are increasing. Figure 4.12 shows these facts. For 800 samples we can go back to see Figure 4.5, which also shows similar behavior. If we refer to Table 3.1 for settling time, we can see that during the time of one second none of the modes should have died down, which tells us that there should be enough oscillations captured in the time record of the signal.

From these results we can infer that with increasing time record length, results converge to certain modes. But for a reliable result, there should be enough harmonics present to describe the characteristics of the signal. Again though pretty robust for lower modes (first 4 here).

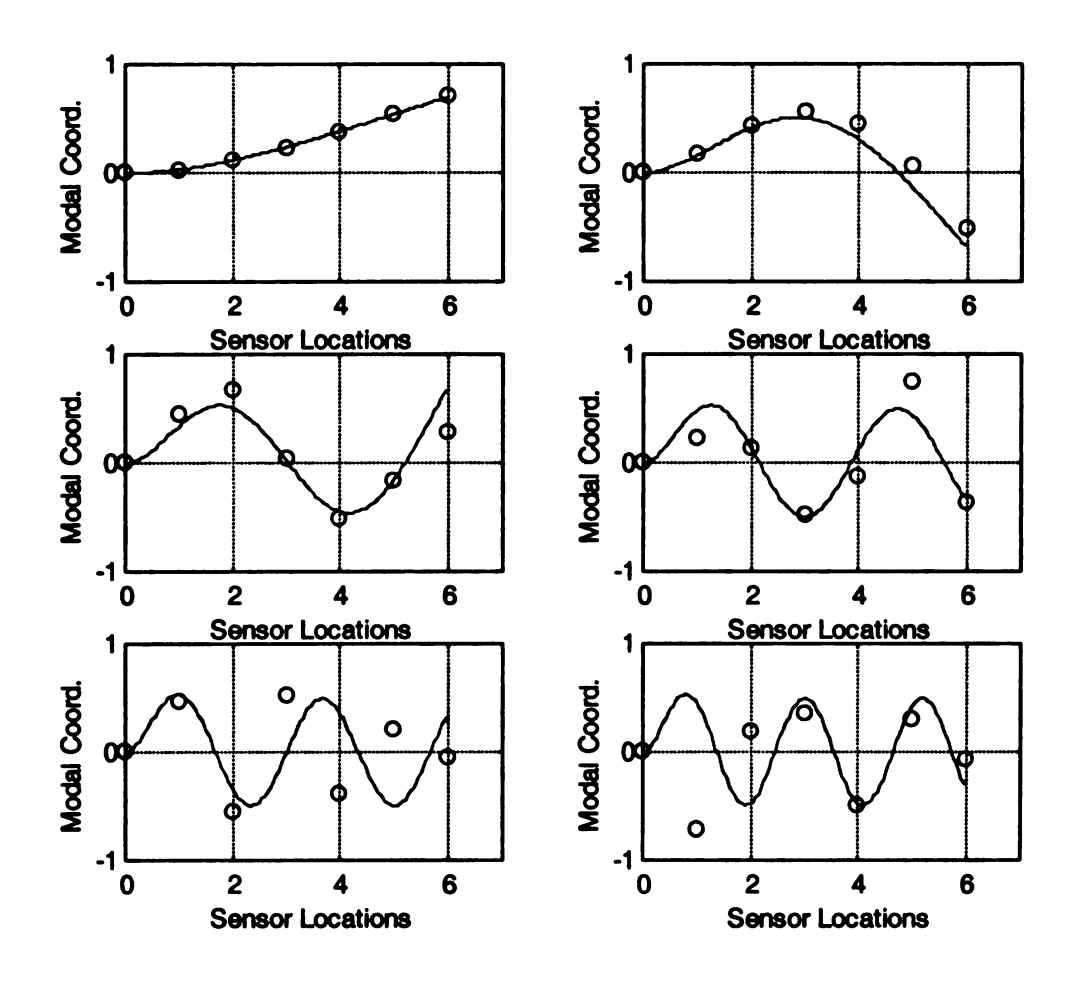


Figure 4.9: Proper orthogonal modes with sampling rate of 800 samples per second and time record length of 0.0075sec. (6 samples)

POMs	$Norm = \ \phi_n - \nu\ $	POVs
1	0.02293	0.2391
2	0.3127	6.0648× 10 ⁻⁴
3	0.4671	1.5042× 10 ⁻⁶
4	0.4954	1.0023× 10 ⁻⁸
5	1.2651	1.3219× 10 ⁻¹¹
6	1.3115	3.6267× 10 ⁻¹⁰

Table 4.9: Norm of error with LNMs for each mode and their corresponding proper orthogonal values for sampling rate of 800 samples per second.

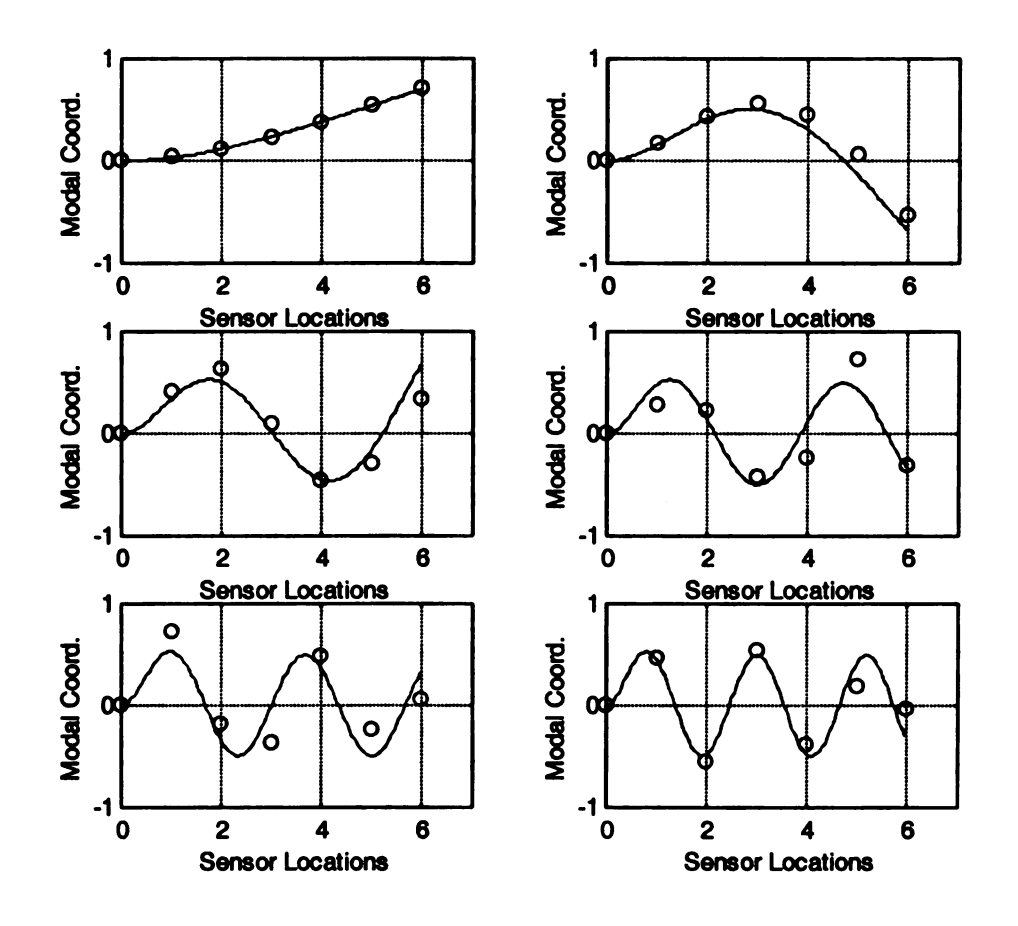


Figure 4.10: Proper orthogonal modes with sampling rate of 800 samples per second and time record length of 0.025 sec. (20 samples)

POMs	$\mathbf{Norm} = \left\ \phi_n - \nu \right\ $	POVs
1	0.0167	0.3736
2	0.3081	7.4483×10^{-3}
3	0.4325	2.6055× 10 ⁻⁵
4	0.5537	3.6777× 10 ⁻⁷
5	0.6288	3.2394× 10 ⁻⁹
6	0.3917	2.4802×10^{-10}

Table 4.10: Norm of error with LNMs for each mode and their corresponding proper orthogonal values for sampling rate of 800 samples per second.

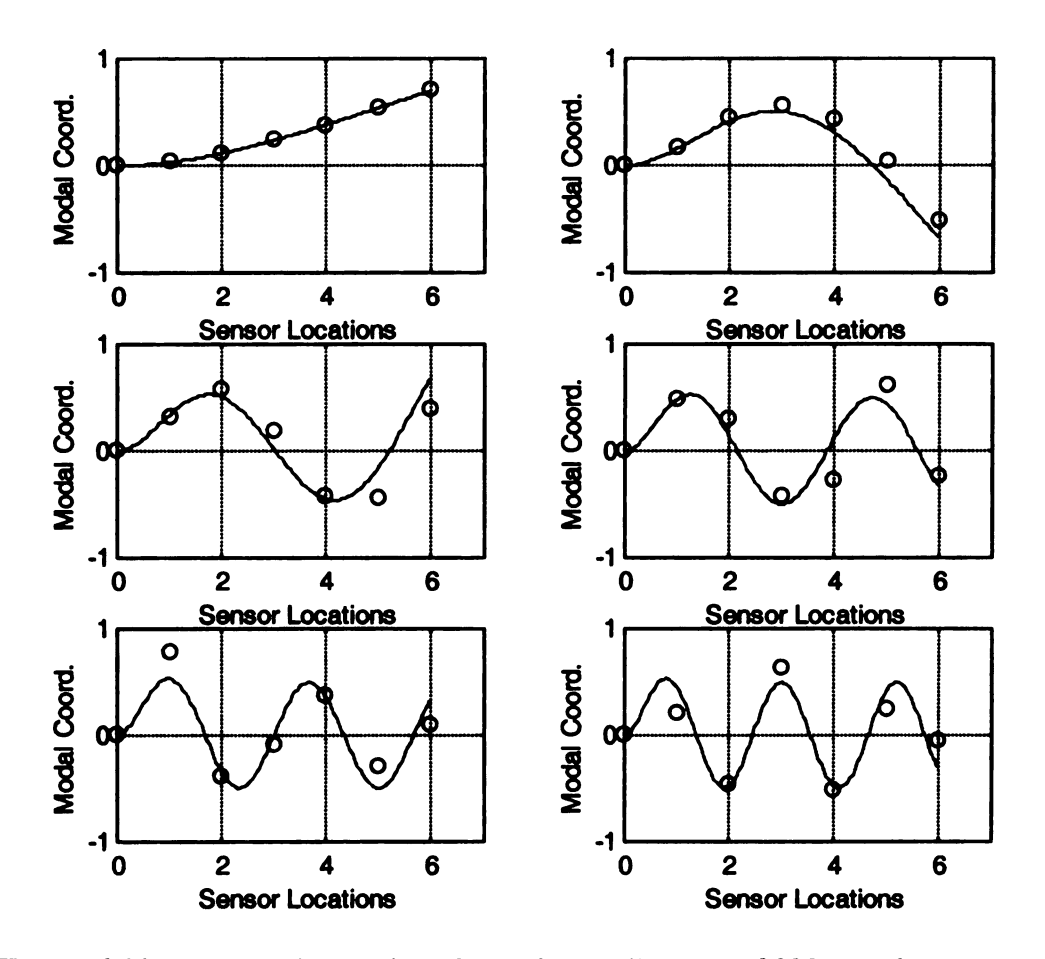


Figure 4.11: Proper orthogonal modes with sampling rate of 800 samples per second and time record length of 0.25 seconds. (200 samples)

POMs	$Norm = \ \phi_n - \nu\ $	POVs
1	0.0106	3.6586
2	0.2972	7.4897×10^{-3}
3	0.4573	3.3040× 10 ⁻⁵
4	0.5052	3.2049× 10 ⁻⁶
5	0.4421	3.2220× 10 ⁻⁸
6	0.4224	1.3198× 10 ⁻⁹

Table 4.11: Norm of error with LNMs for each mode and their corresponding proper orthogonal values for sampling rate of 800 samples per second.

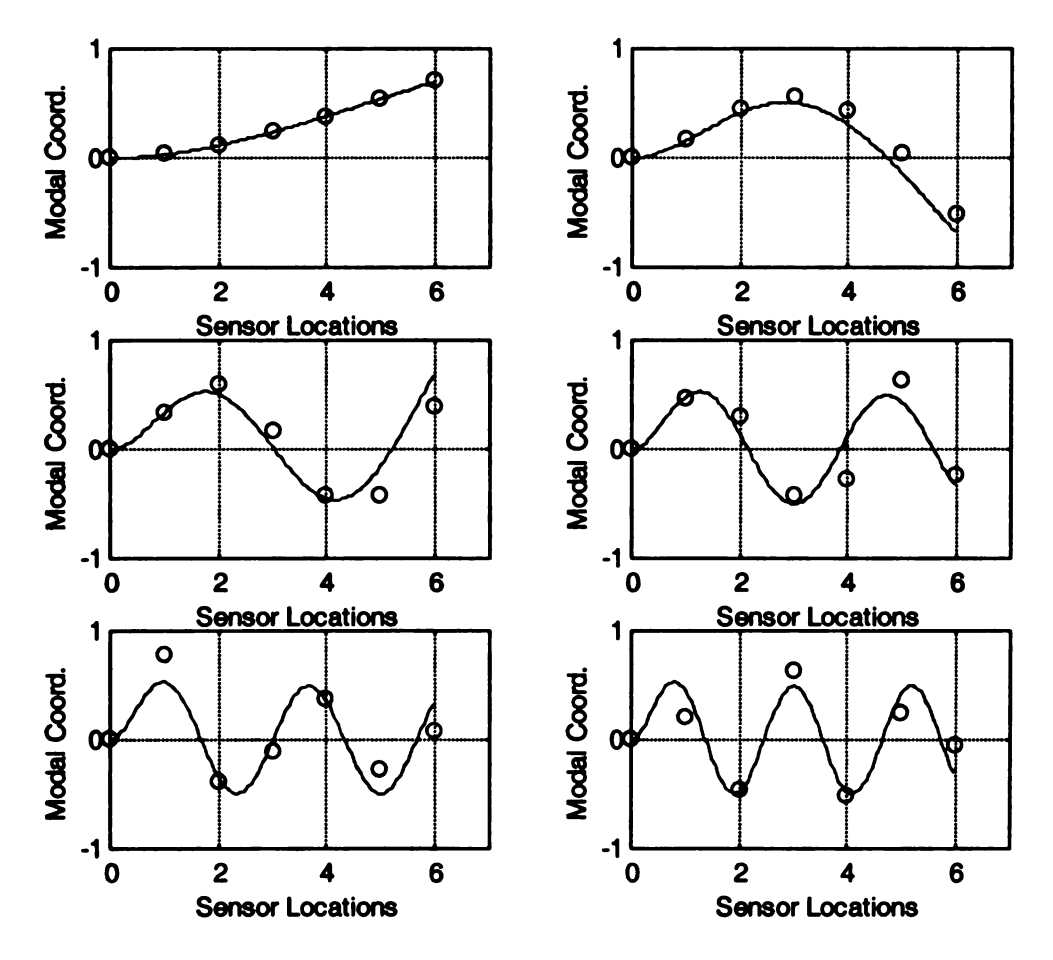


Figure 4.12: Proper orthogonal modes with sampling rate of 800 samples per second and time record length of 0.5 seconds. (400 samples)

POMs	$Norm = \ \phi_n - \nu\ $	POVs
1	0.0105	3.6438
2	0.2976	5.8039×10^{-3}
3	0.4510	2.0844× 10 ⁻⁵
4	0.5030	1.9993× 10 ⁻⁶
5	0.4528	2.6580× 10 ⁻⁸
6	0.4189	1.3646× 10 ⁻⁹

Table 4.12: Norm of error with linear normal modes for each mode and their corresponding proper orthogonal values for sampling rate of 800 samples per second.

4.4 Decomposition of the Strain Signals

In this section we approach the modal analysis through the strain signal and obtain the modes called "strain modes". We discuss the method followed by different experiments performed to obtain these modes. The goal here is to see whether it is feasible to apply POD at various stages of the data-analysis process. Before, we sensed the strains, estimated displacements at various points on the beam, and applied POD to those displacements. The displacements, and hence the modes, are dependent on the basis used for the conversion form strain to displacement. "Strain modes" would be independent of the choice for the basis functions. The question here is whether it is worthwhile to apply POD to strain distribution and then convert strain modes to displacement modes.

4.4.1 Strain Modes

Consider as an example a beam of length 'L'. For normalization of "strain modes" $\psi_i(x) = \phi''(x)$ we can use the inner product of modes $\phi_i(x)$ and $\phi_j(x)$. the if the modes are normalized, we can say

$$\left\langle \phi_{i}, L(\phi_{j}) \right\rangle = \int_{0}^{L} E I \phi_{j}^{-} \phi_{i} dx = \omega_{j}^{2} \delta_{ij}$$

Using integration by parts and boundary conditions listed in section 3.1 we can say

$$\int_{0}^{L} \phi_{i}''(x) \phi_{j}''(x) dx = \alpha_{j} \delta_{ij}$$

$$\alpha_{j} = \frac{\omega_{j}^{2}}{E I}$$

where

Keeping the section 2.3 in mind, the strain modes $\psi_i(x)$ can be discretized such that

$$\mathbf{w}_{i} = [\psi_{i}(\mathbf{x}_{1}) \dots \psi_{i}(\mathbf{x}_{M})]^{T}$$

Then for an equally spaced strain distribution, the orthogonality condition using rectangular rule is

$$W_i^T W_j = \sum_{k=1}^M \psi_i(x_k) \psi_j(x_k) \approx \left(\frac{1}{h}\right) \int_0^L \psi_i(x) \psi_j(x) dx$$

where h is the spacing of spatial discretization. But the problem arises here is that the distribution of strain along the length is not even. To over come this problem we can try two options.

- 1. Try weighted POD to account for $h_{end} > h_s$ (to be developed)
- 2. Assumption of strain as nearly zero at the free end region

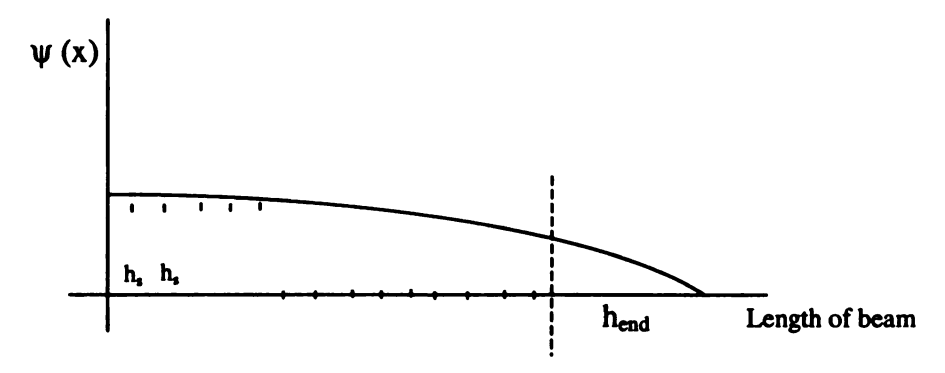


Figure 4.13 Strain distribution along the length of beam

We tried the second option in our tests. If the strain is taken at 'M' different locations on the beam then at any time 't', then the strain values are

$$s_1(t), \, s_2(t), \, s_3(t), \, \, , \, s_M(t)$$

If we collect N times samples we can form a strain-history vector as

$$\mathbf{s}_{i}(t) = [S_{i}(t_{1}), S_{i}(t_{2}), S_{i}(t_{3}), \dots, S_{i}(t_{N})]^{T}$$
 $i = 1, 2, \dots, M$

An NxM ensemble strain matrix can be formed as

$$S = [s_1, s_2, s_3, s_4, \dots, s_M]$$
 N×M size matrix

In the above we have arranged the matrix such that each column represents the strain at M points at any instant of time. A correlation matrix can be made as

$$R_s = \frac{1}{N} S^T S$$

Now we will convert the strain correlation modes to displacement form so that we can compare it with the normal modes. Say we have six modes from above correlation as j_1 , j_2 , j_3 , j_4 , j_5 , j_6 . We can convert each modal vector to displacement vector using modal basis formula

$$d_i = \phi_i(x) \psi_i^{-1}(x) j_i$$

where $\phi_i(x)$ form a basis satisfying the geometric conditions and

$$\psi_i(x) = \frac{\partial^2 \phi_i(x)}{\partial x^2}$$

4.4.2 Experimentation and results

We tried this technique for finding strain modes for our cantilever beam. First attempt was made with strain correlation modes, and found the strain modes as shown in Figure 4.14 and Table 4.13. Only the dominant mode with maximum energy is comparable. The second try to improve the results was done manipulating strain correlation modes. As the strain at the free end of cantilever is zero, so the last entry of

each mode was made zero to see the effect. The results are present in Figure 4.15 and Table 4.14. Here the results did not showed a lot of improvements. The main reason behind the improper results is the uneven distribution of strain. So we can say that it works well if the interest is in the dominant mode only. Whether it works for a uniform strain distribution remains to be seen.

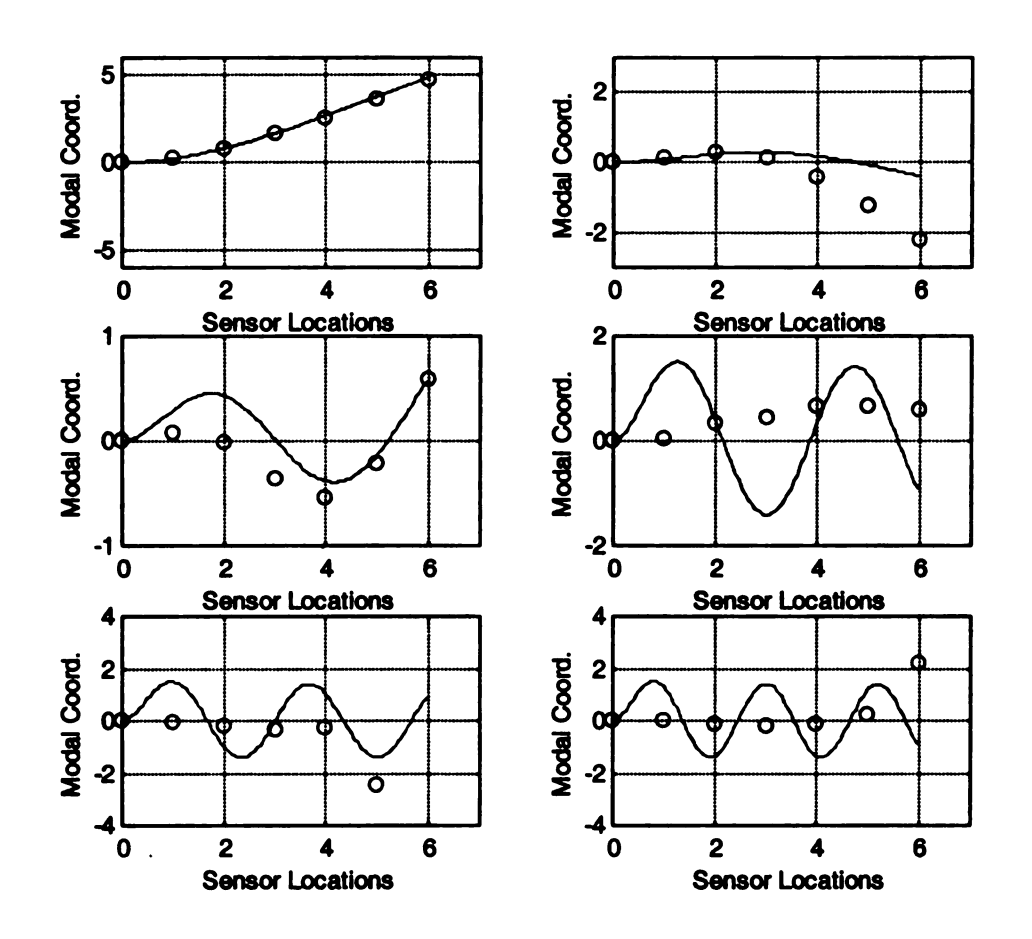


Figure 4.14: Displacement modes converted from strain modes with sampling rate of 800 samples per second and input applied between 3rd and 4th strain gage.

SMs	$Norm = \ \phi_n - \nu\ $	SPOVs
1	1.7003	2.5430
2	1.5335	6.1103×10 ⁻¹
3	1.7525	1.7074× 10 ⁻²
4	1.5881	1.0379× 10 ⁻⁴
5	1.1984	3.4607× 10 ⁻⁵
6	1.4358	1.7909× 10 ⁻⁴

Table 4.13: Norm of error with linear normal modes for each mode and their corresponding strain POVs for sampling rate of 800 samples per second.

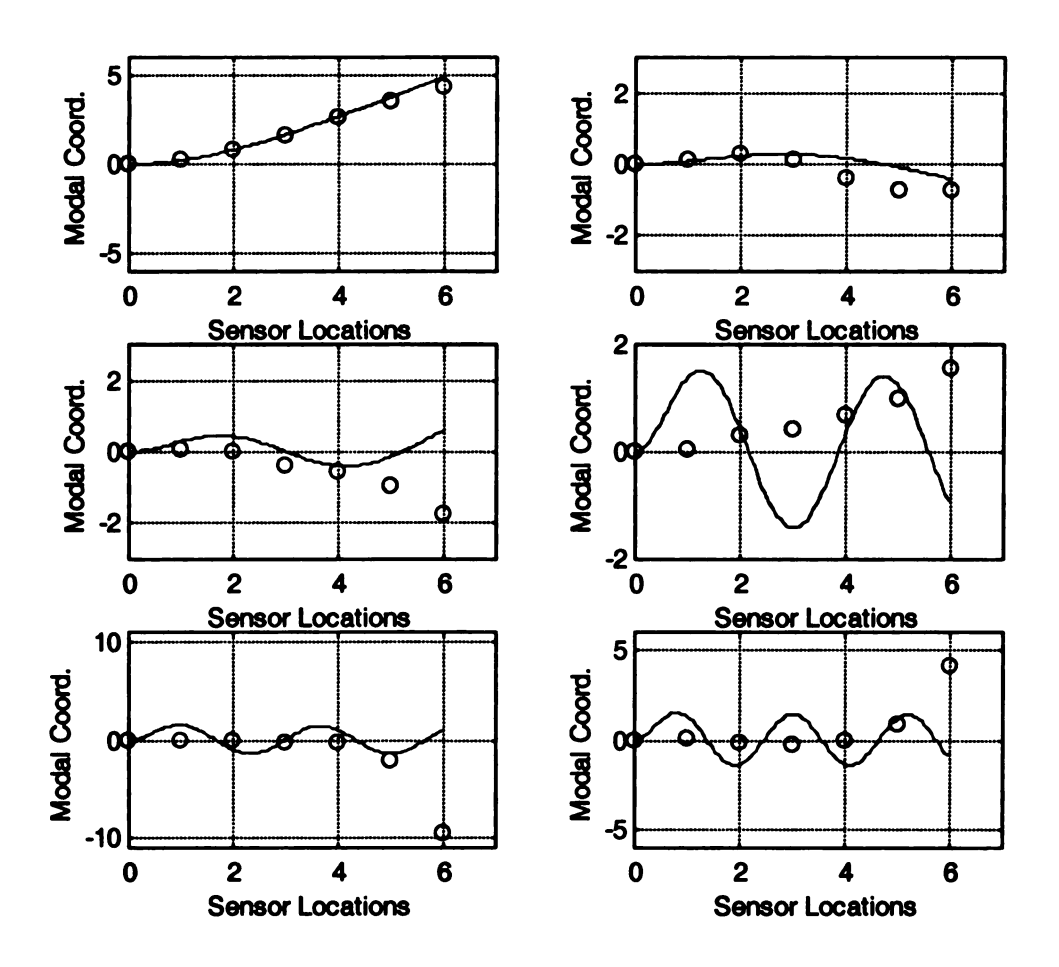


Figure 4.15: Displacement modes converted from strain modes with sampling rate of 800 samples per second and input applied between 3rd and 4th strain gage for zero end strain correlation vectors.

SMs	$Norm = \ \phi_n - \nu\ $	SPOVs
1	1.6592	2.5430
2	1.3294	6.1103× 10 ⁻¹
3	1.5101	1.7074× 10 ⁻²
4	1.5274	1.0379× 10 ⁻⁴
5	1.2816	3.4607× 10 ⁻⁵
6	1.5669	1.7909× 10 ⁻⁴

Table 4.14: Norm of error with linear normal modes for each mode and their corresponding strain POVs for sampling rate of 800 samples per second.

4.5 POMs based on a large number of "pseudo sensors"

Until now POMs were determined using six sensors. The conversion from strain to displacement information was done for discrete locations by using the first six LNMs. We are extending this idea to generate a large number of "pseudo sensors" on the beam. Here, we evaluate the linear normal modal functions at 21 different locations thereby yielding 21 pseudo displacement sensors, separated by 0.0197m on a cantilever of length 0.3937m. However, as we used only first six LNMs to curve fit, the system measurement only contains six independent displacements.

The motive for using the pseudo sensors is to improve the resolution associated with the rectangular rule integration that effectively underlies the relationship between orthogonality of linear normal modal functions, orthogonality between discrete POMs and the uniformly discretized modal vector. The six LNMs (or basis functions in general) in some way provide a smoothing interpolation for the numerical integration. Kappagantu [5] had previously used Gramm-Schmitt orthonormalization when converting from discrete POMs to continuous "proper orthogonal modal function". Evidence indicated that the pseudo sensors performed an equivalent task. However, this interpolation depends on the interpolating functions and how well they depict the physics of the problem.

Using these pseudo sensors we obtained displacements at 21 equi-distant points along the whole length of the beam. We applied this idea to three different tests to check the validity of this concept. Figure 4.16 to 4.18 shows the POMs obtained using pseudo

sensors. A general observation from these plots is that the continuous version of the dominant modes tend to the orthonormalized functions with increasing number of sensors. A comparison can be made by looking at the Figure 4.5 - 4.7 of the same configurations with six sensors.

In this case, the quality of the results may be a reflection of the fact that our basis consists of the LNMs. With the pseudo sensors, we are effectively interpolating between sensors with the ideal interpolating functions. Testing with other choices of basis functions will be done in the next section.

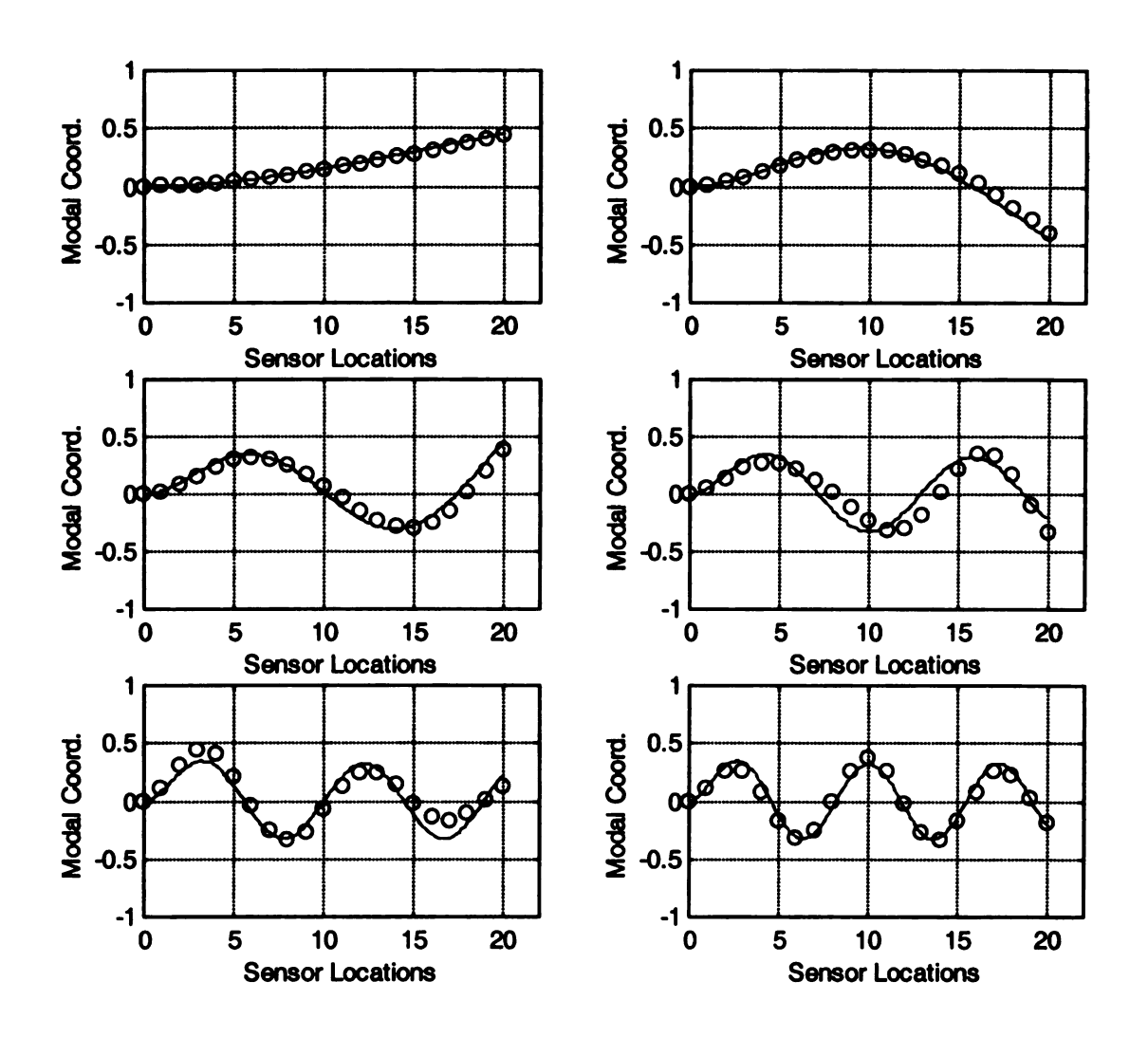


Figure 4.16: Proper orthogonal modes with sampling rate of 800 samples per second and input applied between 4th and 5th strain gage using 21 pseudo sensors.

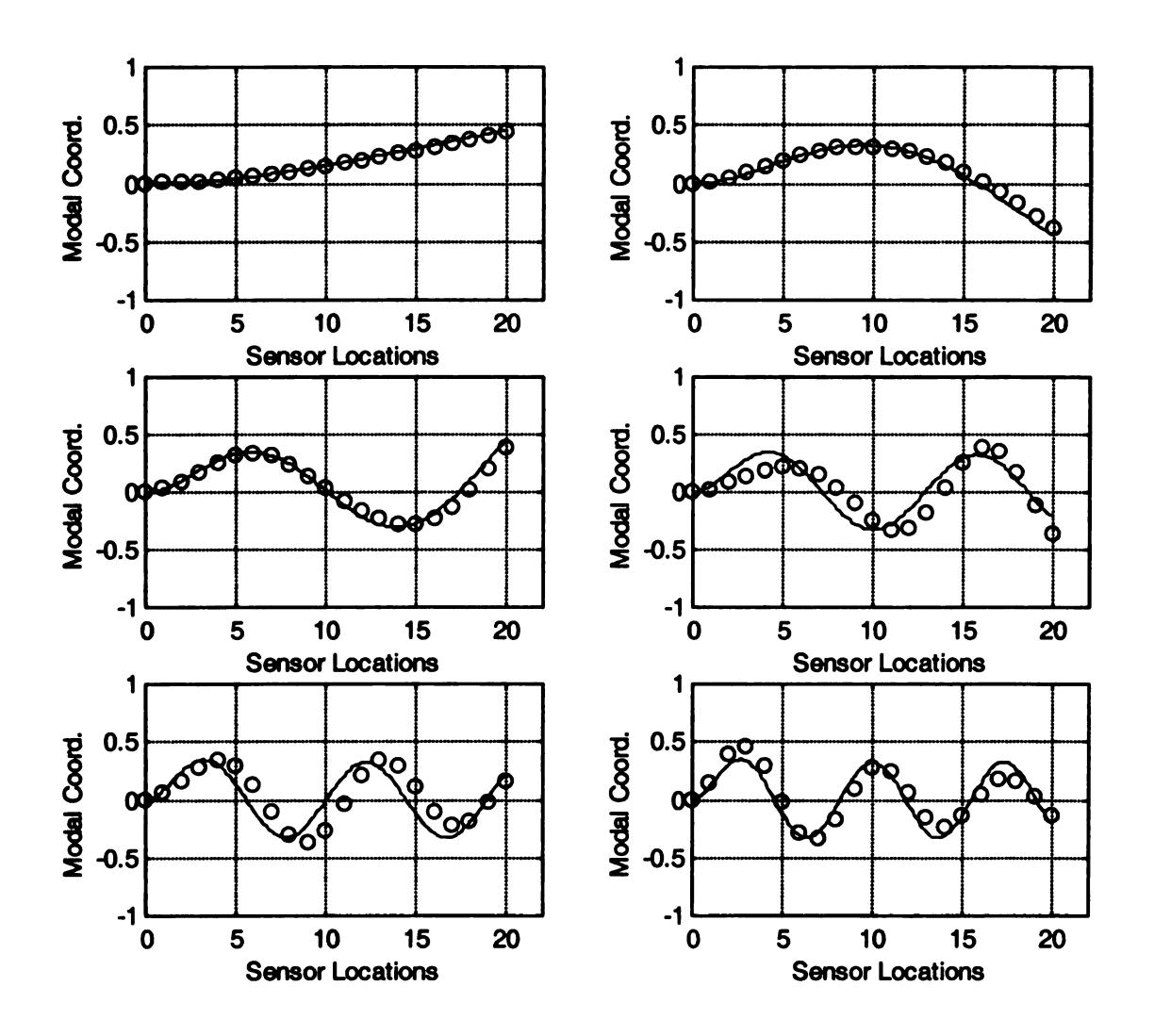


Figure 4.17: Proper orthogonal modes with sampling rate of 800 samples per second and input applied between 3rd and 4th strain gage using 21 pseudo sensors.

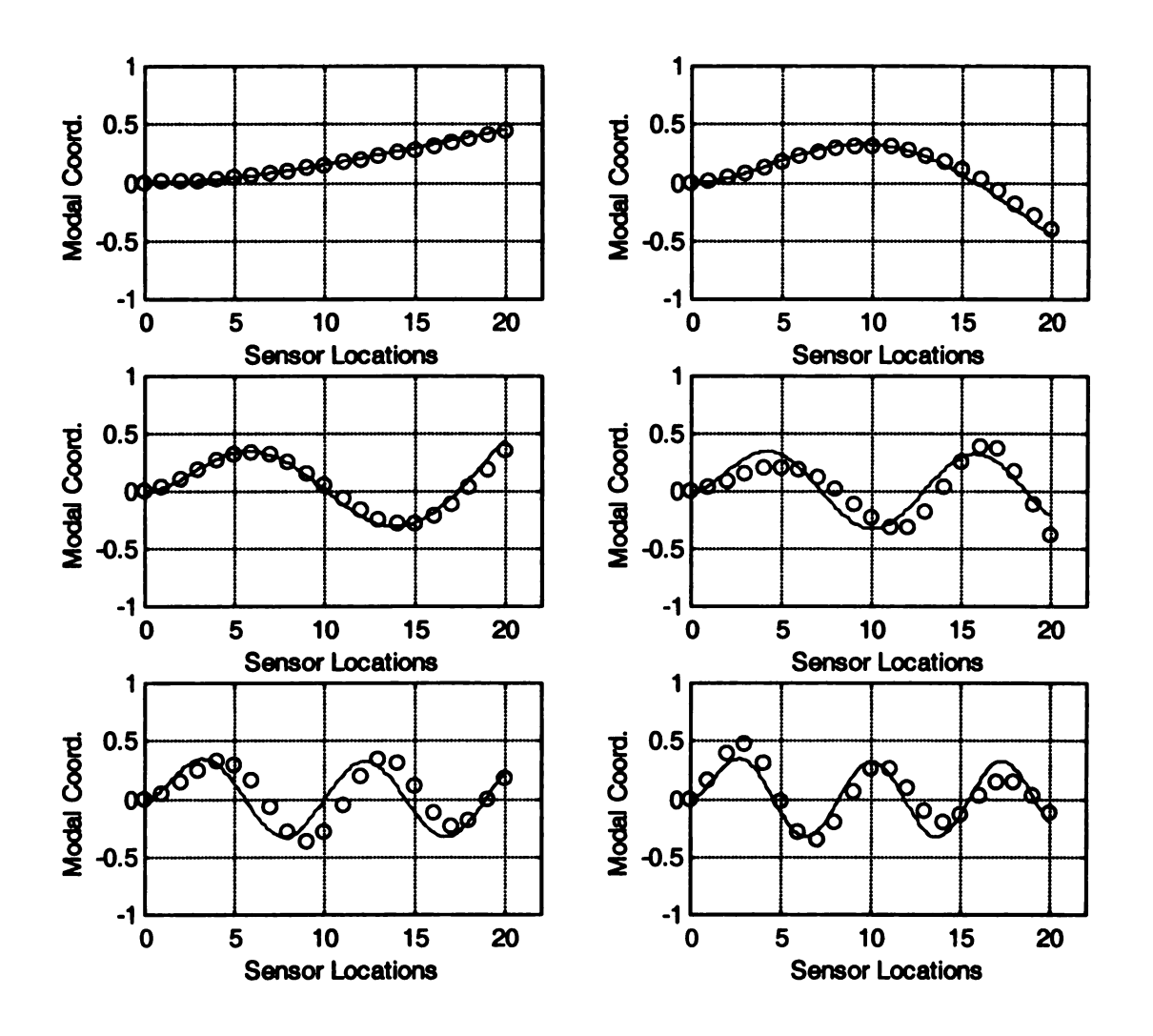


Figure 4.18: Proper orthogonal modes with sampling rate of 800 samples per second and input applied between 2nd and 3rd strain gage using 21 pseudo sensors.

4.6 POD with Admissible Basis functions

Up to now we have been blessed with an orthonormal basis which is composed of LNMs of the model. Typically, the LNMs of the model will not be available; indeed the model itself may not be available. In such case we need to choose a set of basis functions which differ from the real modes. In the following, we use two other sets of orthonormal basis to see if our pervious results have been positively biased due to LNMs as a basis.

In the field of vibrations we define two classes of functions. The functions satisfying the entire boundary conditions of the problem and can carry P derivatives, are referred to as the class of comparison functions, where P is the order of the self-adjoint operator L in the governing equation of motion of the system. The other class is called the admissible functions. These are functions which satisfy only the geometric boundary conditions of the problem and can carry P/2 derivatives. The comparison functions are by definition admissible functions, and in fact they constitute a small subset of the much larger class of admissible functions.

We selected two sets of basis functions which satisfy our geometric boundary conditions. The first one is as follows:

$$f_1(x) = x^2$$

$$f_2(x) = x^2 + a x^3$$

$$f_3(x) = x^2 + b x^3 + c x^4$$

$$f_4(x) = x^2 + d x^3 + e x^4 + f x^5$$

$$f_5(x) = x^2 + g x^3 + h x^4 + i x^5 + j x^6$$

$$f_6(x) = x^2 + k x^3 + m x^4 + n x^5 + o x^6 + p x^7$$

The values of constants a, b,..., p were found using an inner product over the whole length of beam to make each function orthogonal to all others. So for the value of 'a',

using first two basis functions, we used
$$\int_{0}^{0.3937} f_1(x) f_2(x) dx = 0$$

Similarly for 'b' and 'c', using first three equations to form two algebraic equations by making $f_3(x)$ orthogonal to $f_1(x)$ and $f_2(x)$. For our beam of length 0.3937 m, we found the values of the constants as

$$a = -3.04801$$
, $b = -7.11201$, $c = 12.043$, $d = -12.192$, $e = 46.4517$, $f = -56.1846$, $g = -18.288$, $h = 116.129$ $i = -132.015$, $j = 294.337$, $k = -25.4001$, $m = 236.56$, $n = -1030.05$, $o = 2125.77$, $p = -1679.83$.

We used this set of admissible functions as basis functions for POD process. In first experiment, the data was taken at the rate of 800 samples/second. The input was given at the free end, so the excitation of first mode is expected to be higher. The results showed that POMs roughly approximate LNMs. The energy distribution also shows maximum energy in the first mode. The results can be seen in Figure 4.19 and Table 4.15. In the second test, data were taken at a sampling rate of 1000 samples/second with input at the free end. Figure 4.20 and Table 4.16 also show the same trend. In Figure 4.21 and Table 4.17 we plotted POMs vs. basis functions to see whether POMs converge to admissible functions. The results show a little different trend from when POMs were compared with LNMs. Comparing Figures 4.19 and 4.21, the norm of error is decreased when POMs are compared with basis functions. The behavior of the curves at the end in plots can be regarded as the characteristics of admissible functions.

We applied the idea of pseudo sensors (section 4.5) to see whether the dominant modes tend to the orthonormalize with increasing number of sensors. Figures 4.22 and 4.23 clearly show the validity of this idea. So we can say that with increasing number of sensors, it allows the rectangular integration to increase resolution, hence leading to better approximation. In these plots we can see that endpoint of POMs show different behavior from rest of points. This can be due to the properties carried by the basis functions. Curiously, if we omit the few end data point pseudo sensors, POMs 3, 4, 5 and 6 otherwise seem to match LNMs 2, 3, 4 and 5 respectively. We increase the number of pseudo sensors from 21 to 41 to see the effect on the endpoints of POMs. Figure 4.24 show that with increasing number of sensed data the modes converges more towards LNMs.

As a conclusion we can say that the basis functions have a significant influence on the results. The POMs are distorted from LNMs compared to earlier examples. The pseudo sensors may help a little, but not greatly.

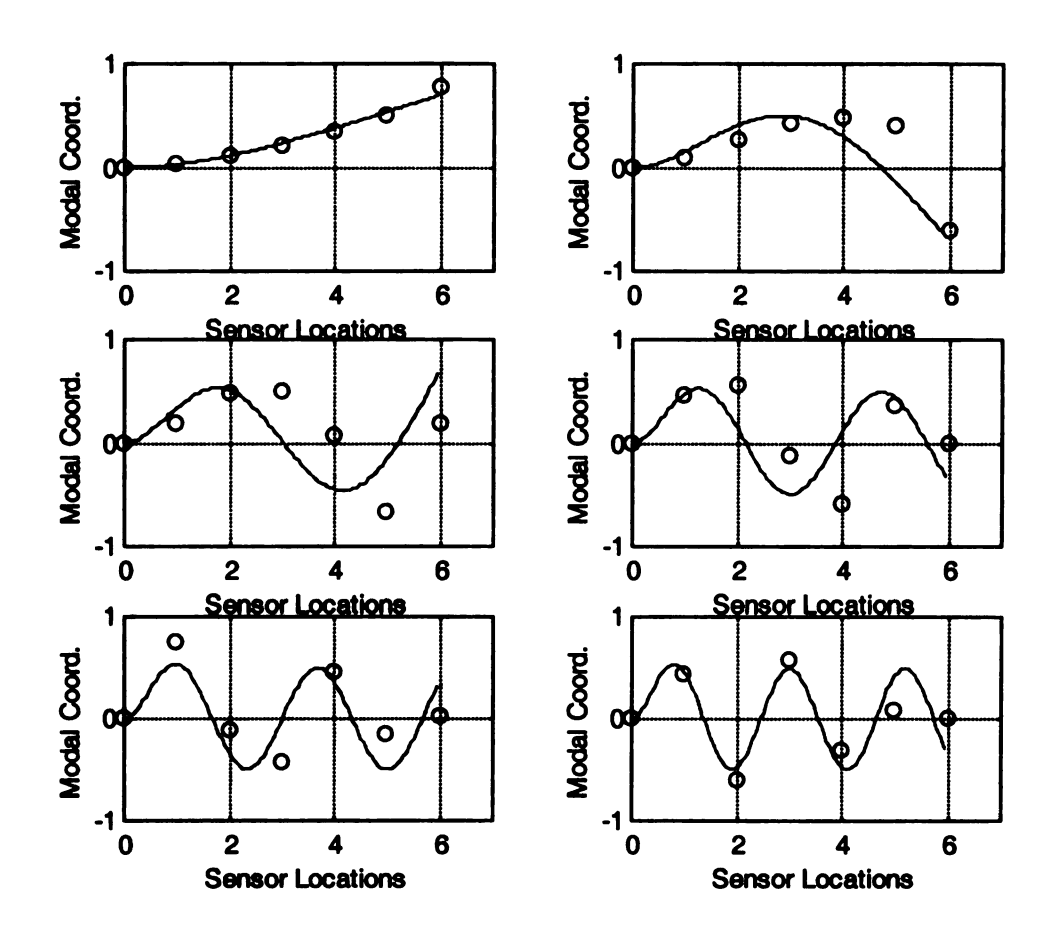


Figure 4.19: Proper orthogonal modes with sampling rate of 800 samples per second using 1st set of admissible functions (—— show the LNMs).

POMs	$\mathbf{Norm} = \left\ \phi_n - \nu \right\ $	POVs
1	0.1008	1.8232
2	0.6007	8.6645×10 ⁻⁴
3	1.0102	3.1630× 10 ⁻⁵
4	1.0211	5.0322× 10 ⁻⁷
5	0.7488	5.0314× 10 ⁻⁸
6	0.5091	4.8254× 10 ⁻⁹

Table 4.15: Norm of error with 1st set of admissible functions for each mode and their corresponding proper orthogonal values for sampling rate of 800 samples per second.

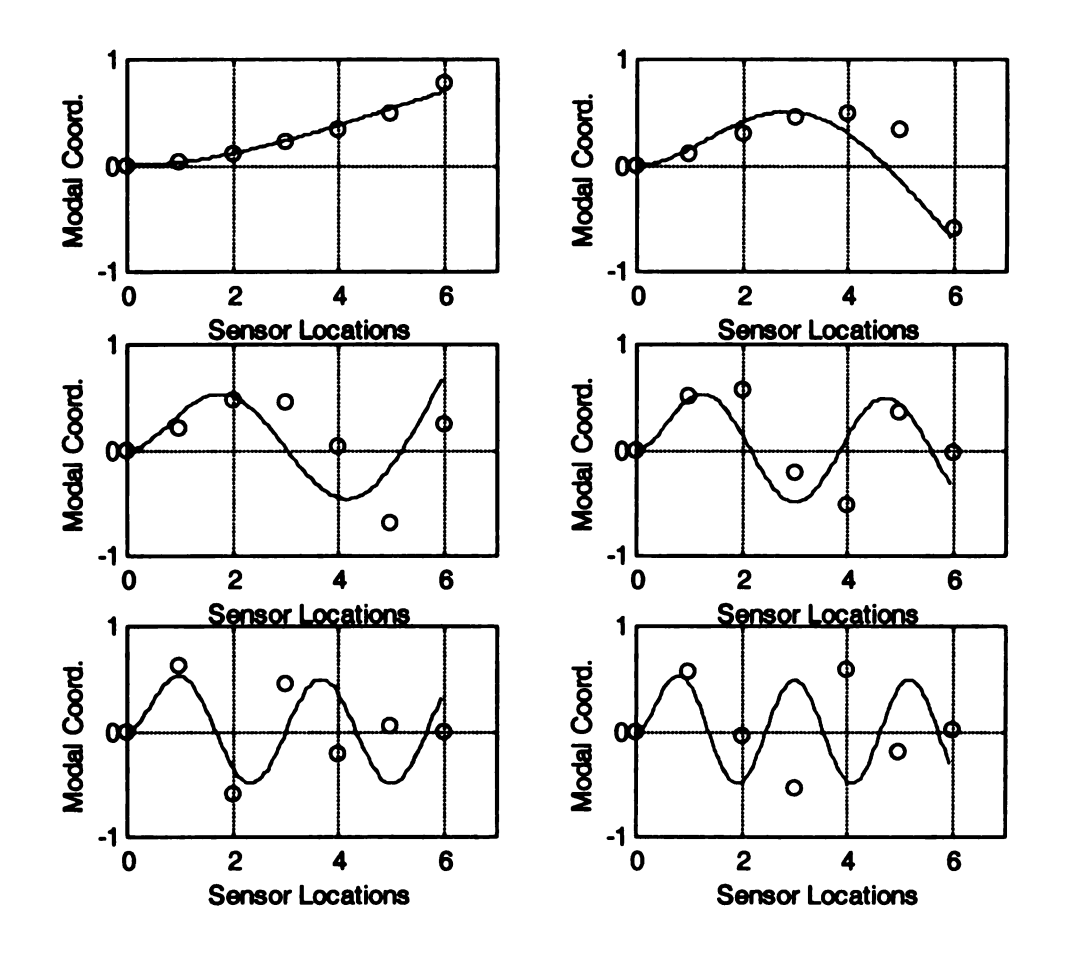


Figure 4.20: Proper orthogonal modes with sampling rate of 1000 samples per second using 1st set of admissible functions (— show the LNMs).

POMs	$Norm = \ \phi_n - \nu\ $	POVs
1	0.1030	2.2951
2	0.5440	5.2711×10 ⁻³
3	0.9546	1.0876×10 ⁻⁴
4	0.9307	3.4825× 10 ⁻⁶
5	1.0345	1.3127× 10 ⁻⁸
6	1.1585	4.0077× 10 ⁻⁷

Table 4.16: Norm of error with 1st set of admissible functions for each mode and their corresponding proper orthogonal values for sampling rate of 1000 samples per second.

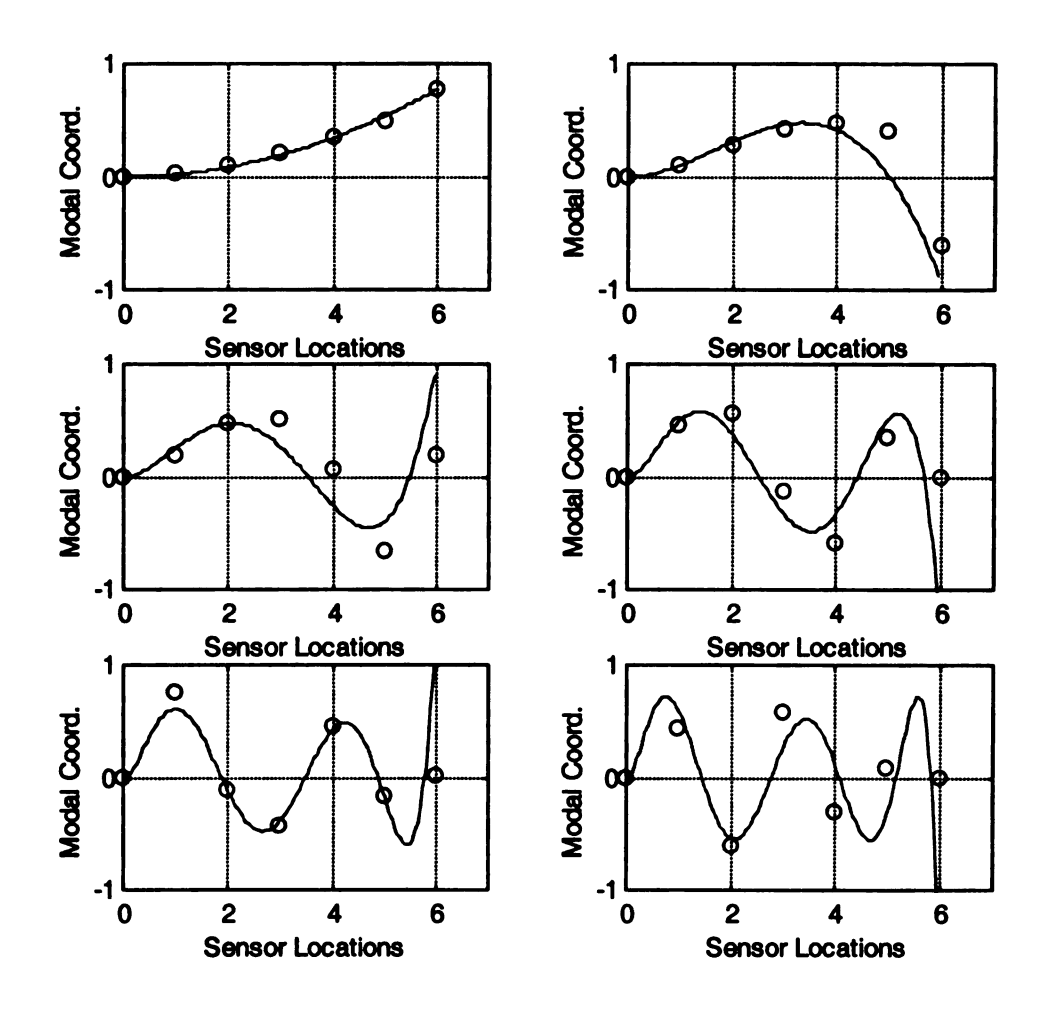


Figure 4.21: Proper orthogonal modes with sampling rate of 800 samples per second using 1st set of admissible functions (—— show the Basis function).

POMs	$Norm = \ \phi_n - \nu\ $	POVs
1	0.04864	1.8232
2	0.4513	8.664× 10 ⁻⁴
3	0.8245	3.1631× 10 ⁻⁵
4	0.9648	5.0322× 10 ⁻⁷
5	1.7457	5.0314× 10 ⁻⁸
6	1.1304	4.8254× 10 ⁻⁹

Table 4.17: Norm of error with 1st set of admissible functions for each mode and their corresponding proper orthogonal values for sampling rate of 800 samples per second.

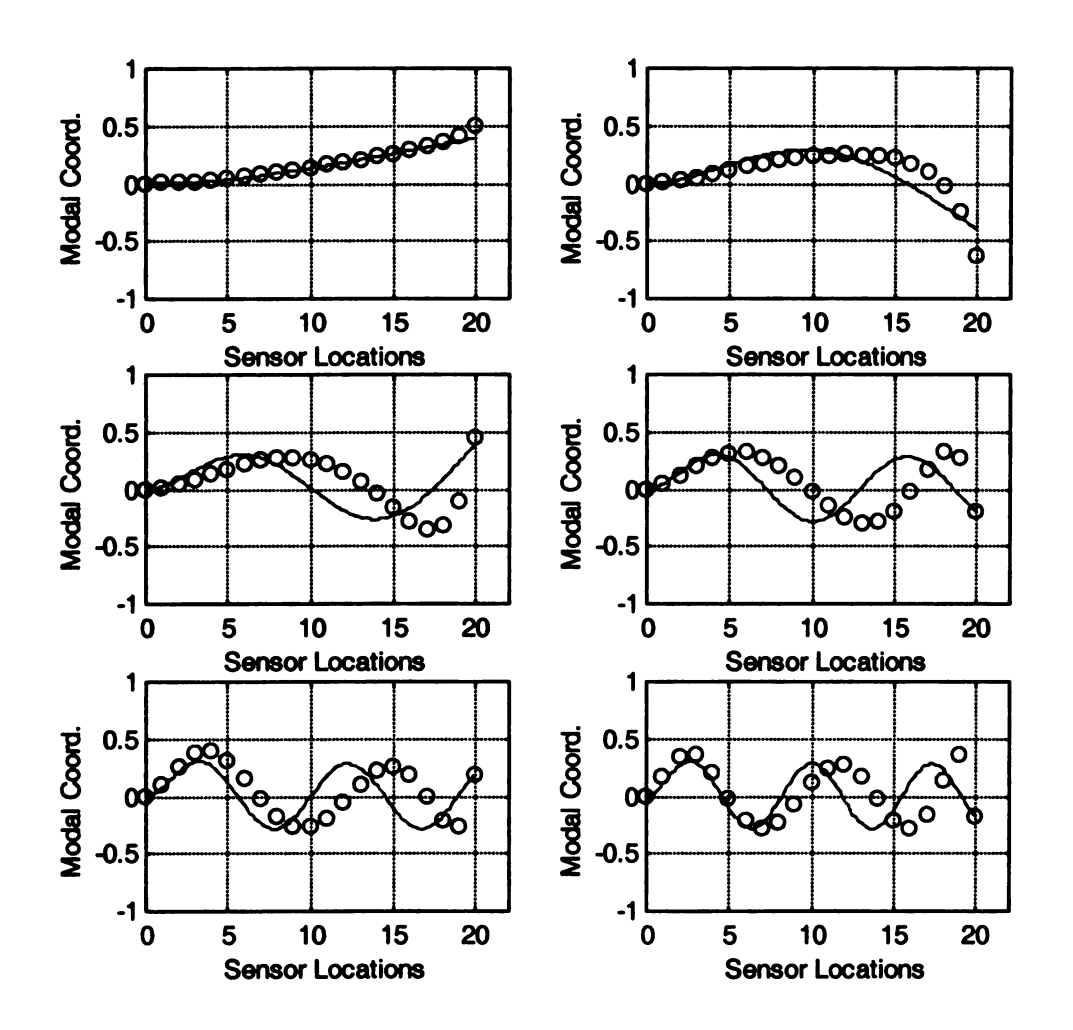


Figure 4.22: Proper orthogonal modes with sampling rate of 800 samples per second using 1st set of admissible functions with 21 pseudo sensors

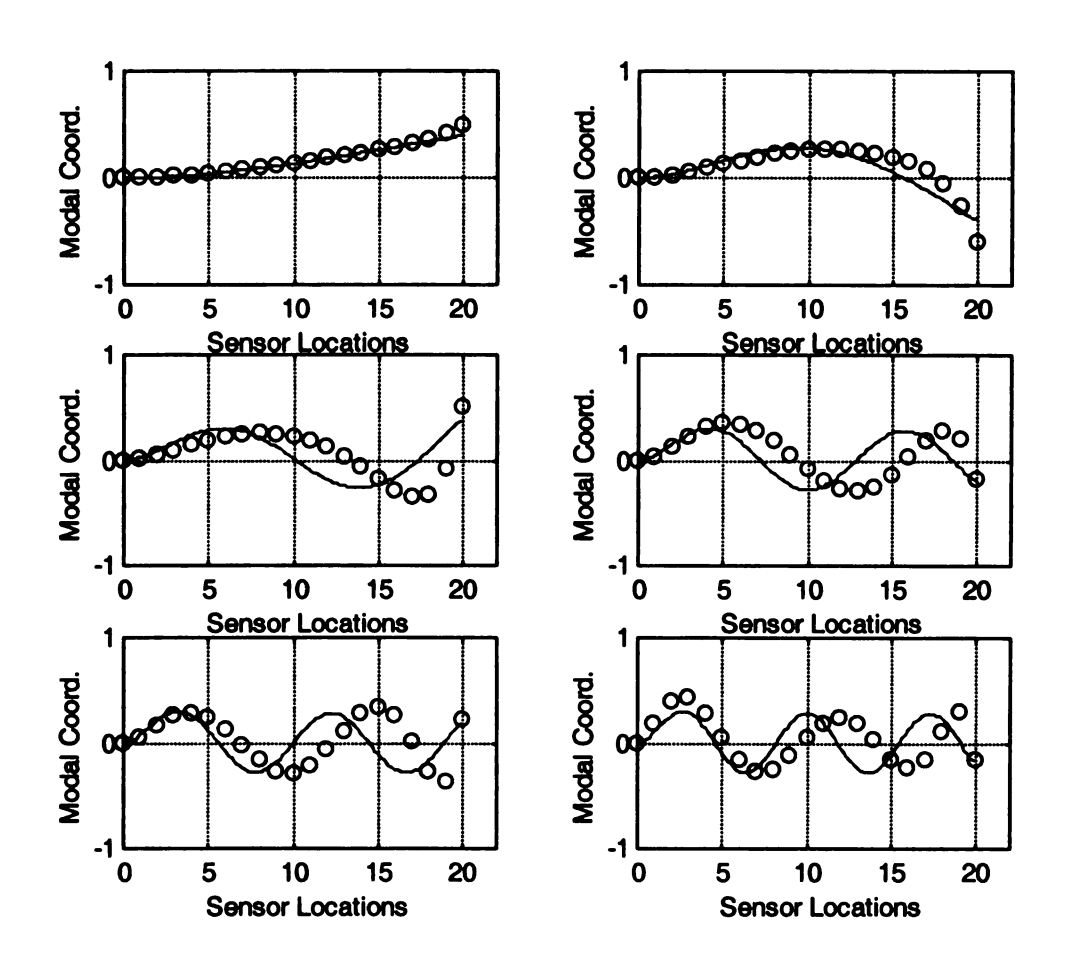


Figure 4.23: Proper orthogonal modes with sampling rate of 1000 samples per second using 1st set of admissible functions with 21 pseudo sensors

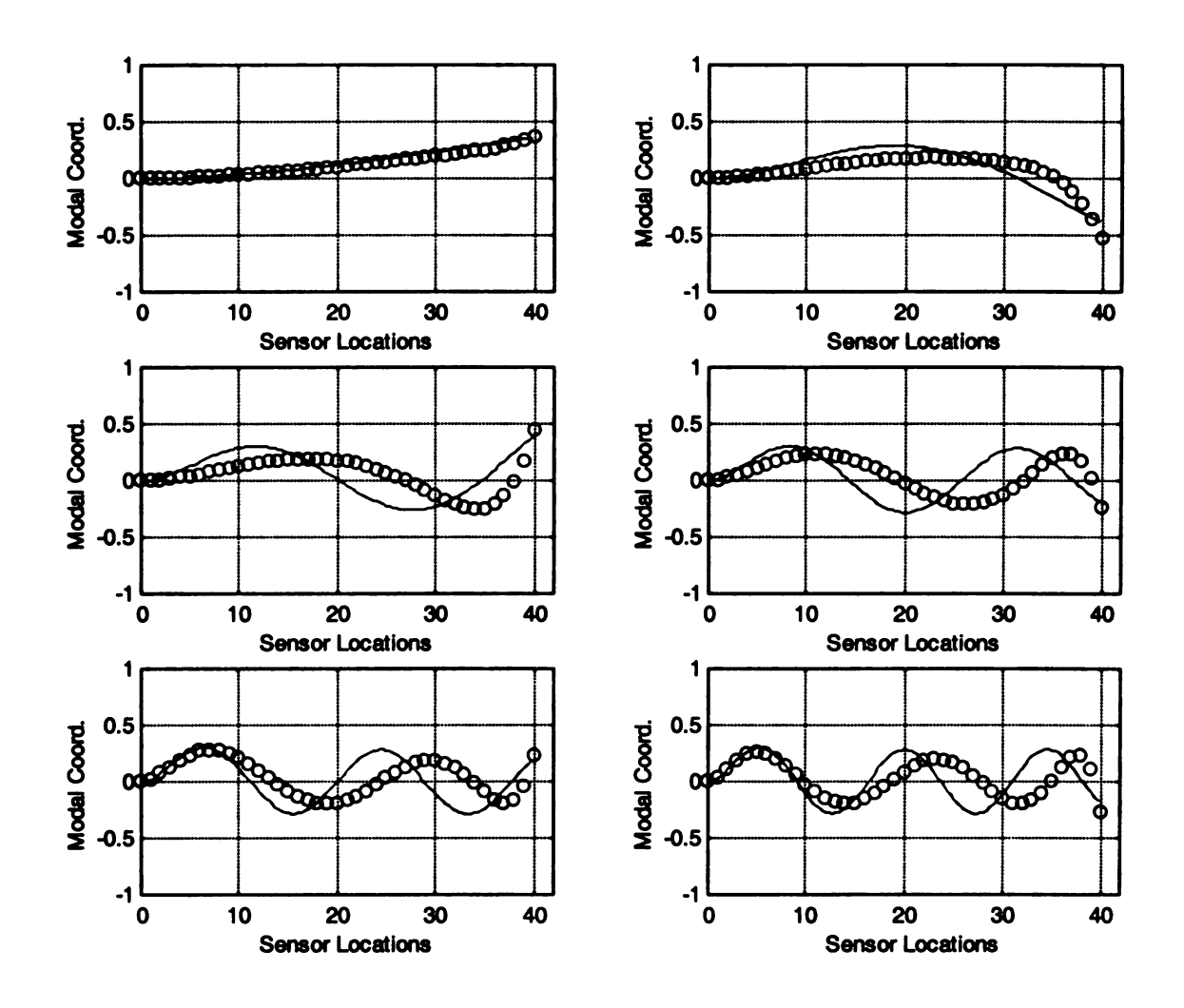


Figure 4.24: Proper orthogonal modes with sampling rate of 800 samples per second using 1st set of admissible functions with 41 pseudo sensors

The second set of admissible functions used is

$$f_1(x) = 1 - Cos\left(\frac{\pi}{2l}x\right)$$

$$f_2(x) = 1 - Cos\left(\frac{3\pi}{2l}x\right)$$

$$f_3(x) = 1 - Cos\left(\frac{5\pi}{2l}x\right)$$

$$f_4(x) = 1 - Cos\left(\frac{7\pi}{2l}x\right)$$

$$f_5(x) = 1 - Cos\left(\frac{9\pi}{2l}x\right)$$

$$f_6(x) = 1 - Cos\left(\frac{11\pi}{2l}x\right)$$

We used this set of admissible functions as basis functions for POD process.

These functions satisfy the geometric boundary conditions, and also one of the natural boundary conditions, that of zero curvature at the end of the beam. While these functions are independent, they are not orthogonal. The same tests were repeated by using same data, to compare the results of both sets of functions. The results with 800 samples/second data are quite encouraging and can be seen in Figure 4.25 and Table 4.18. But there is little difference in results, between the first and second set of admissible functions, which can be due to improper selection of admissible functions or on the other hand the problem of not acquiring data precisely. But the overall picture of the system behavior is acceptable. The first mode is carrying the maximum energy of the system. For the second test with 1000 samples the results are at Figure 4.26 and Table 4.19.

The pseudo sensor idea is also applied here. The results here are more appreciable with increasing number of sensors. Figures 4.27 and 4.28 give the plots showing improved resolution and modes converging to LNMs. We can also compare that the resolution in the case of 2nd set of admissible functions is more than the first set.

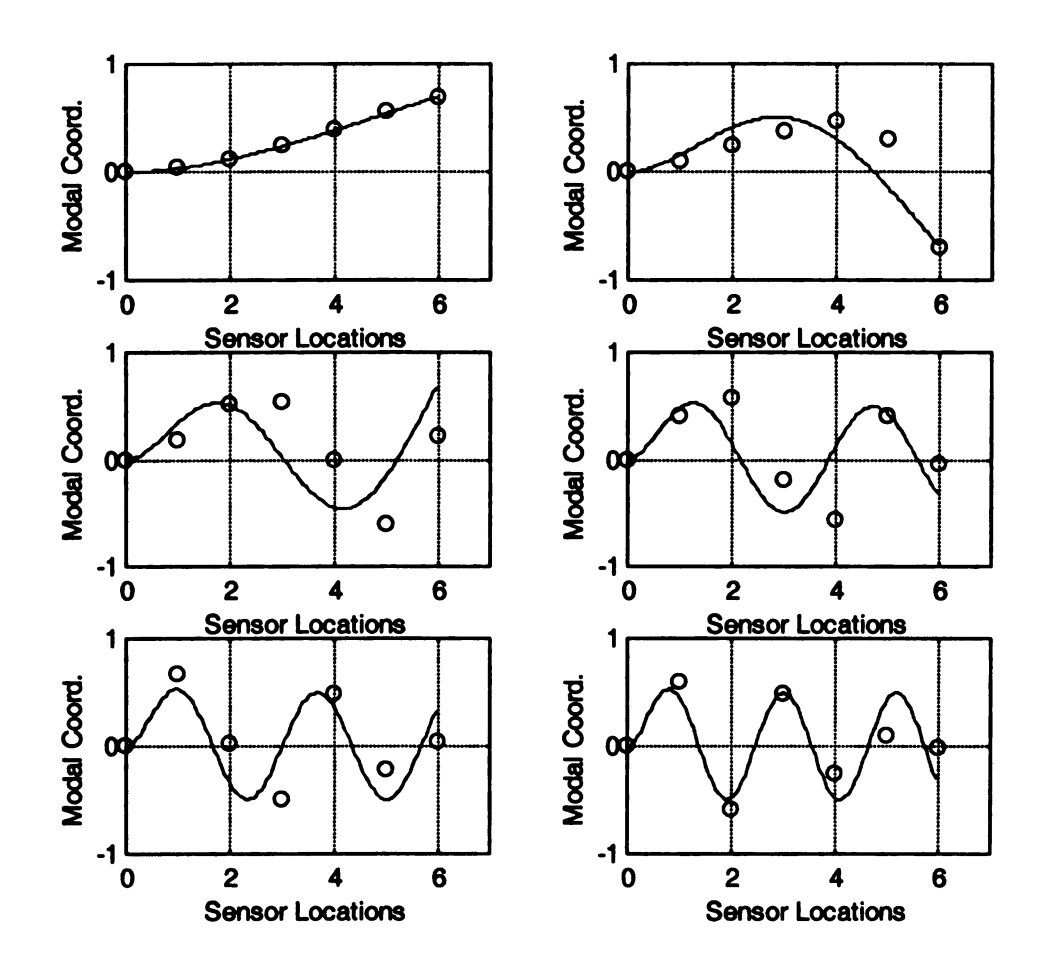


Figure 4.25: Proper orthogonal modes with sampling rate of 800 samples per second using 2nd set of admissible functions.

POMs	$Norm = \ \phi_n - \nu\ $	POVs
1	0.0296	1.3411
2	0.5265	1.3005× 10 ⁻³
3	0.9533	2.9207× 10 ⁻⁵
4	0.9639	3.3137×10^{-7}
5	1.0965	1.2567× 10 ⁻⁸
6	1.2060	1.9617× 10 ⁻⁹

Table 4.18: Norm of error with 2nd set of admissible functions for each mode and their corresponding proper orthogonal values for sampling rate of 800 samples per second.

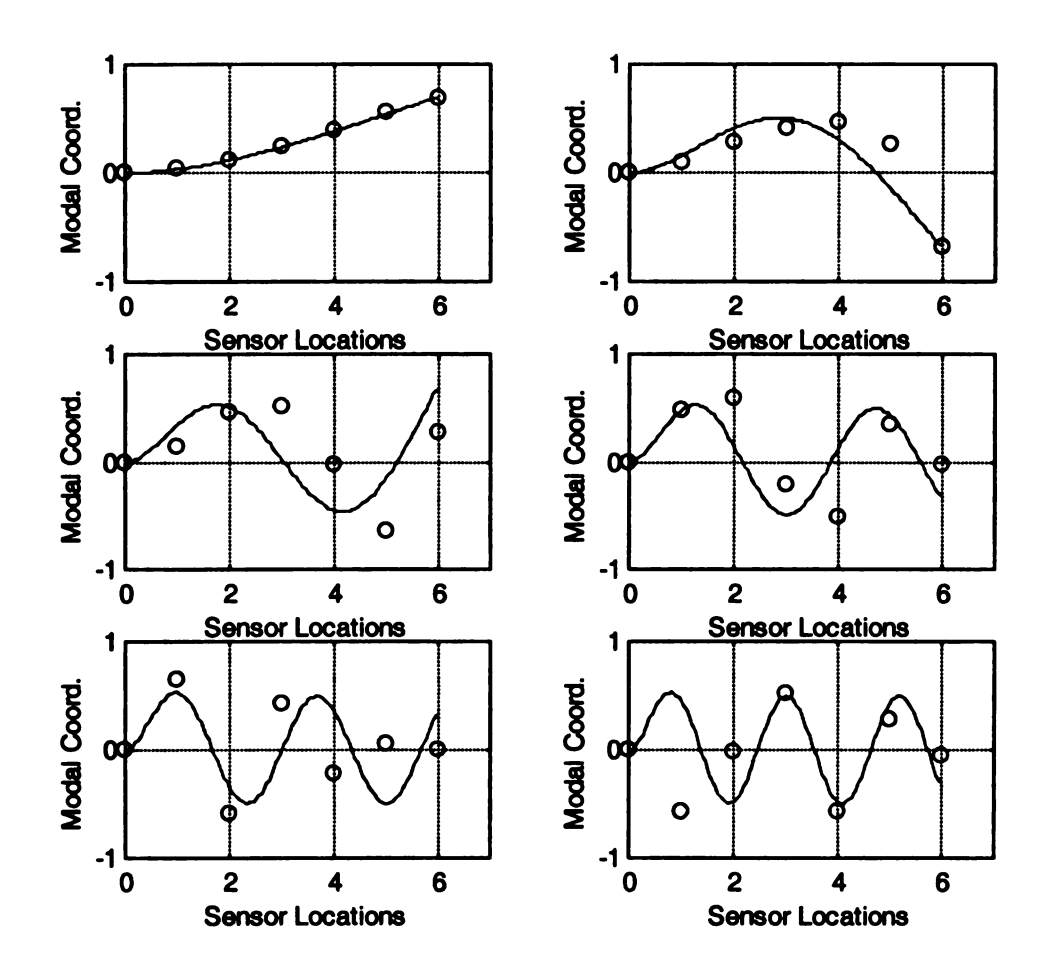


Figure 4.26: Proper orthogonal modes with sampling rate of 1000 samples per second using 2^{nd} set of admissible functions.

POMs	$Norm = \ \phi_n - \nu\ $	POVs
1	0.0263	1.689
2	0.4668	7.4224×10^{-3}
3	0.9396	8.1780× 10 ⁻⁵
4	0.9307	2.1515× 10 ⁻⁶
5	1.0325	4.5328× 10 ⁻⁹
6	1.1086	1.6436× 10 ⁻⁷

Table 4.19: Norm of error with 2nd set of admissible functions for each mode and their corresponding proper orthogonal values for sampling rate of 1000 samples per second.

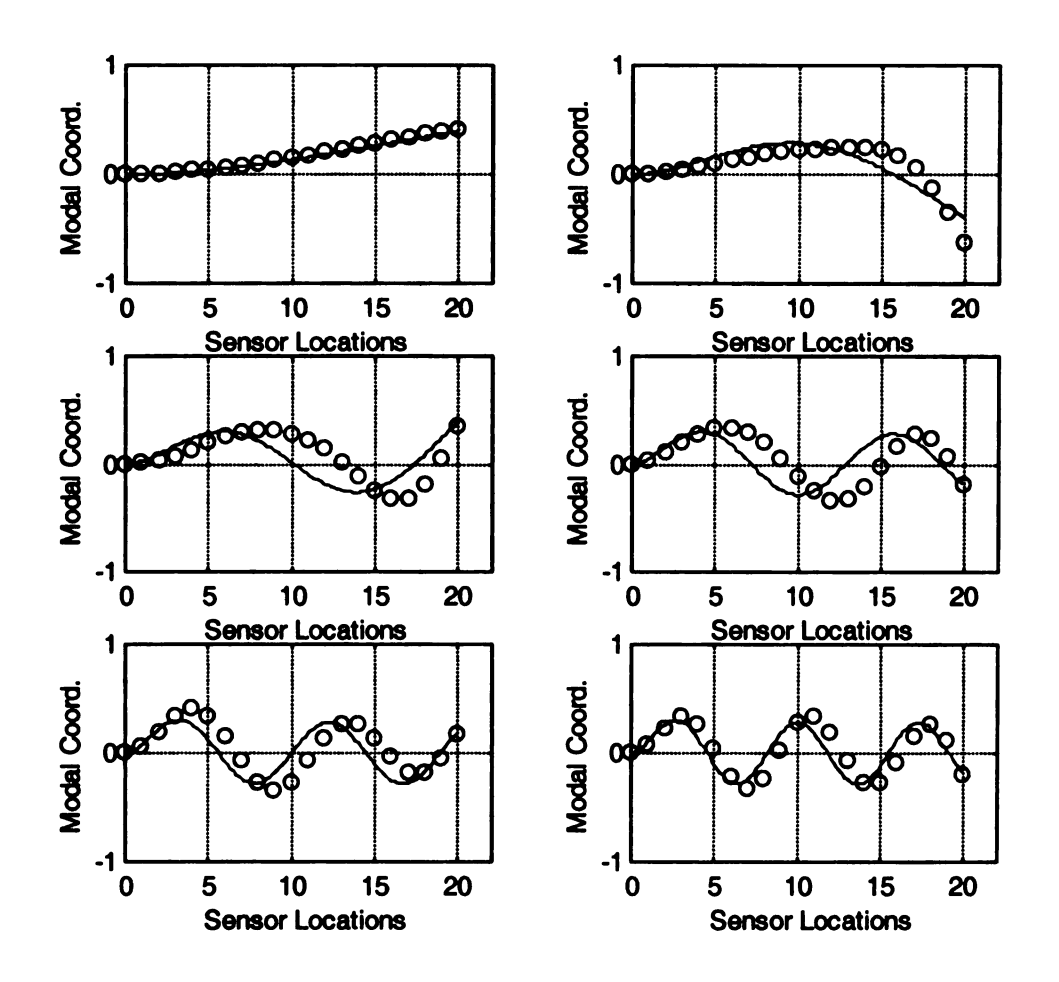


Figure 4.27: Proper orthogonal modes with sampling rate of 800 samples per second using 2nd set of admissible functions with 21 pseudo sensors

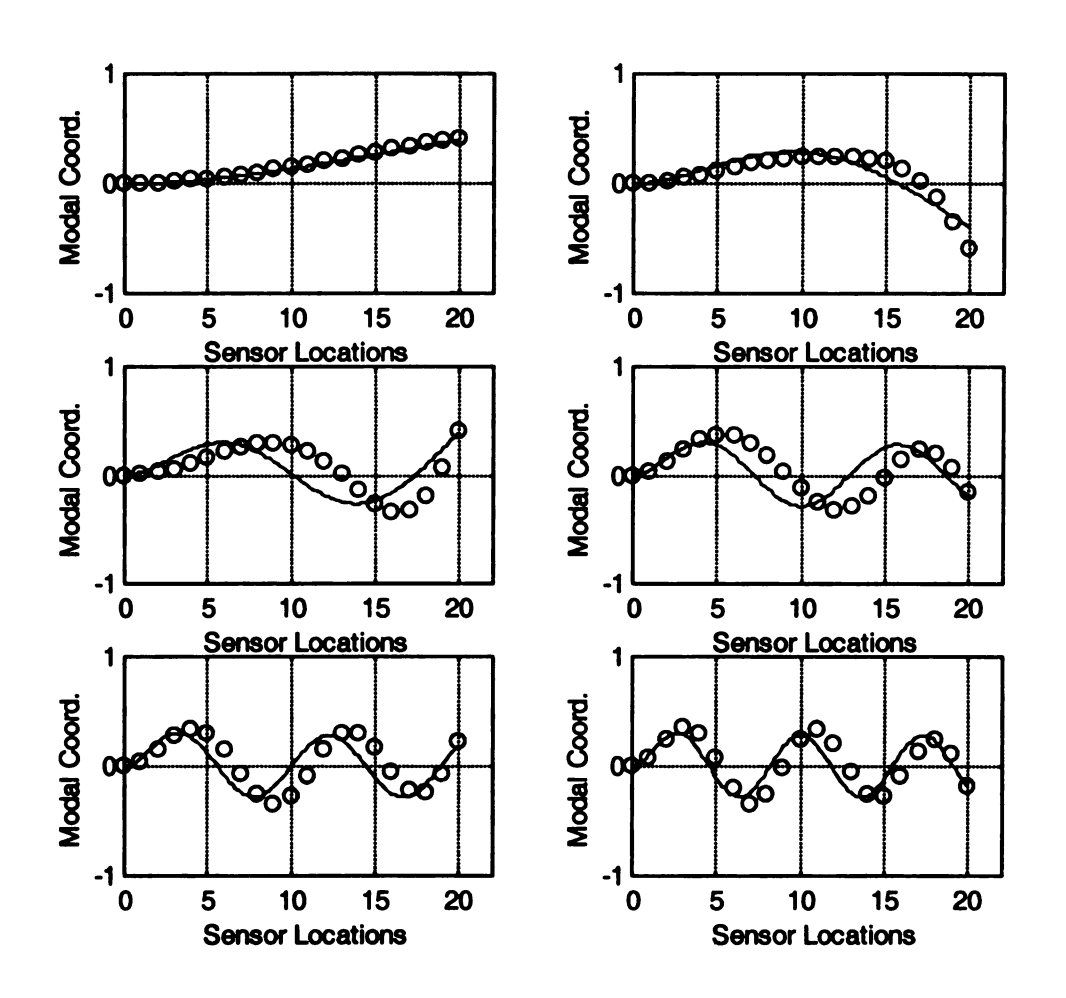


Figure 4.28: Proper orthogonal modes with sampling rate of 1000 samples per second using 2nd set of admissible functions with 21 pseudo sensors

Chapter 5

Conclusions

5.1 Summary of work

In this study, the application of POD as a tool for identifying linear normal modes in distributed parameter systems has been done experimentally. These experiments validate numerical studies done previously. We have shown the ease of use of this method and compared the results with LNMs.

First we summarized the theory behind the proper orthogonal decomposition to understand the previous work. To obtain experimental modes, we used a cantilever with strain gages. The six strain gages restricted us to six identified modes. Simple bending theory was used to find the relation between strain and displacement. To check the validity of POD, different experimental parameters were varied. Matlab was used for different data manipulations, which were acquired from the cantilever.

5.2 Conclusion

Various experiments were performed to monitor the accuracy and validity of the POD process. The accuracy of results depends upon how accurately the data is acquired.

Reduction of noise, proper interface of hardware elements and quality of software used improves the quality of data acquisition. All the results based on displacements measurements showed that the lower POMs converge to approximately LNMs. For the portion of experiment when the sampling rate was varied, it was observed that the accuracy of results increases somewhat with increasing sampling rates. This is logical in the sense that as more information of a signal is available for a certain period, it is easier to obtain characteristics of the signal. But the most important aspect is to meet the Nyquist criterion to avoid aliasing effects. Overall, this method is quite robust for lower (1-3) modes.

The second portion of the test was to excite different modes by applying input at various locations of the cantilever. As we were not providing the exact initial conditions for any specific mode, no pure mode was excited. We provided impulse input to the system, so higher modes were likely excited. When the input was toward the free end, excitation emphasized the first mode. Similarly when we moved the input towards the fixed end, there was increased excitation of other modes. But in all the cases we saw that maximum energy was with the first mode. When the input was applied near a nodal point, the corresponding mode was excited less. The magnitude of energy was reduced as the other modes were excited more. But there are some modes which always had significant energy in them. We should consider such modes for design and analysis.

For the next tests we varied the time record length of data acquisition. It was found that for a very small time record length, a rough excitation of the system

characteristics can be made. But for a precise result, we should have enough data to get system characteristics accurately. As a conclusion for these tests, we can say that POMs converge to LNMs as time record length increases, and are quite robust for lower modes.

The POMs obtained from the above experiments were quite close to LNMs. We tried to increase the resolution of our results by putting some pseudo sensors in between the real sensors. From different simulations performed, we can conclude that with increasing number of pseudo sensors, the resolution of the results improved, even though these pseudo sensors did not effect the number of independent sensors. But here we were using LNMs as a basis, so it is expected. Generally, increasing the resolution in sensors should improve results since the approximation is limited by the resolution through a rectangular rule integration of the orthogonality property if the basis functions provide good interpolation.

We tried to get "strain modes" and convert them to displacement modes. The objective behind this was to check the feasibility of the application of POD to various stages of the data analysis process. The main problem for this kind of analysis was the uneven distribution of sampled strains along the length of cantilever. The strain at the free end of the cantilever was zero and maximum at the fixed end. We tried to make the end point strain correlation modes zero by putting zero at the end of each mode. This technique seemed to work for dominant modes only. But we were unable to get meaningful results beyond that.

We investigated the usage of various basis functions for the conversion from strain to displacement. The results suggest that the closer the basis are to the real modes, the better the results are. A measurement which does not involve strain-to-displacement conversion may not have this limitation. There are two possible conclusions. One is that the choice of basis functions influences the POMs "seen" in the system. This may be particularly true with the pseudo sensors, where information is fabricated or extrapolated based on the basis. The other possibility is that the LNMs provide the most accurate estimations of actual displacements for any choice of bases, thus leading to more accurate POMs. To clarify this mystery, it would be beneficial to test a system with directly measured displacements.

The difference between theoretical and experimental results can be due to the assumptions made in the original mathematical model, which result in theoretical normal modes. Thus for better results we should build a mathematical model which should closely meet our real beam. Some other reasons for discrepancies can be noise in the signal or improper interface between the hardware elements. But even then we can see encouraging results by using this simple technique to acquire modes of vibrations.

The cost involved in the data acquisition can be regarded as a disadvantage of this process, but it is still better when we compare it with the computational expenses and learning curve associated with the sophisticated and expensive software involved in determining LNMs by traditional methods. The drawback is that the mass distribution must be known.

5.3 Future work

During the course of our research, we found some improvements and extensions that can be done to extend this work further. First of all we put a basic condition of knowing mass distribution for the usage of POD in modal analysis. If by any way we can relax this condition, the application of this method will increase to a vast number of systems. To make our model more solid, we can consider the vibration along the length of the beam. We are unable to get some good results with highly damped systems, as oscillations die down quickly, so some work can be done on that side too. It may turn out that as the applicability expands beyond current limitations, so will the complexity of the method. Perhaps when it is as widely applicable as conventional modal analysis techniques, it will no longer offer any advantage in terms of simplicity.

It would also be beneficial to extend applicability to uneven sensor distributions. This may require a weighted version of POD. In order to increase the accuracy of results, a more accurate data acquisition hardware system can help. In order to make it a more sound procedure some experiments should be done using other type of beams.

Another area worth investigation are experiments with direct displacement sensors. Such experiments will factor out limitations that depend on the choice of basis functions. It could be important to directly compare POD with conventional model analysis. We could do this with a stiffer system in which an impulse hammer would provide a clean input signal at all locations on the beam. Finally, it would be beneficial to extend the idea in this work to two-dimensional problems such as plates and shells.

With this we conclude our thesis.

Bibliography

- [1] B. Feeny and R. Kappagantu, On the Physical Interpretation of Proper Orthogonal Modes in Vibrations. Journal of Sound and Vibration, 211(4), 607-616, 1998.
- [2] Brian Feeny, Interpreting Proper Orthogonal Modes in Vibrations. In proceedings of DETC'97. ASME Design Engineering Technical Conference. CD-Rom. 1997.
- [3] G. Berkooz, P. Holmes, and J. L. Lumley, *The Proper Orthogonal Decomposition* in the Analysis of Turbulent Flows. In Annual review of Fluid Mechanics, volume 25. Annual Review Inc., New York, 1993.
- [4] D. J. Inman, Engineering Vibration. Prentice Hall, Englewood Cliffs. New Jersey.
- [5] R. Kappagantu V., An Optimal Modal Reduction of Systems with Frictional Excitation, Ph.D. thesis, Michigan State University, 1997.
- [6] J. P. Cusumano and B. Y. Bai, Period-Infinity Periodic Motions, Chaos and Spatial Coherence in a 10 Degree of Freedom Impact Oscillator. Chaos, Solitons and Fractals, 3(5): 515-535, 1993.
- [7] J.P. Cusumano, M. T. Sharkady, and B. W. Kimble. Experimental Measurements of Dimensionality and Spatial Coherence in the Dynamics of a Flexible-Beam Impact Oscillator. Philosophical Transactions of Royal Society of London, 1994.
- [8] Philip M. Fitzsimons and Chunlei Rui, Determining Low Dimensional Models of Distributed Systems. Advances in robust and Nonlinear Control Systems, ASME DSC, 53:9-15,1993.

- [9] Kevin D. Murphy, Using the Karhunen-Loeve Decomposition to Examine Chaotic Snap-Through Oscillations of a Buckled Plate. In Proceedings in Sixth Conference on Nonlinear Vibrations, Stability and Dynamics of Structures, Virginia, June 1996.
- [10] S. R. Sipcic, A. Benguedouar, and A. Pecore, Karhunen-Loeve Decomposition in Dynamical Modeling. In Proceedings in Sixth Conference on Nonlinear Vibrations, Stability and Dynamics of Structures, Virginia, June 1996.
- [11] B. Ravindra, Comments on "On the Physical Interpretation of Proper Orthogonal Modes in Vibrations". Journal of Sound and Vibration, 219(1) 189-192, 1999.
- [12] Jen, C. W., Johnson, D. A. and Dubious F, Numerical Modal Analysis of Structures Based on the Revised Sub-Structure Synthesis Approach, Journal of Sound and Vibration, 180,185-203,1995.
- [13] B. Ravindra, Use of Invariant Measure of Chaotic Attractors in Identification of Vibrating Systems, Presented in the GAMM conference, Regenburg, March 1997.
- [14] M.A. Davies and F.C. Moon, Solution, Chaos and Modal Interactions in Periodic Structures, Nonlinear Dynamics, The Richard Rand 50th Anniversary Volume, pp159-143, edited by A Guran, 1997.
- [15] M.F.A. Azeez and A. F. Vakakis, *Using Karhunen-Loeve Decomposition to Analyze the Vibroimpact Response for a Rotor*, Seventh Conference on Nonlinear Vibrations, Stability, and Dynamics of Structures, Blacksburg, Virginia, July 1998.
- [16] X Ma, M.F.A. Azeez and A. F. Vakakis, Nonparametric, Nonlinear System

 Identification of a Nonlinear Flexible System using Proper Orthogonal

- Decomposition, Seventh Conference on Nonlinear Vibrations, Stability, and Dynamics of Structures, Blacksburg, Virginia, July 1998.
- [17] K. Yasuda and K. Kamiya, Experimental Identification Technique of Nonlinear

 Beams in the Time Domain. 1997 ASME Design Engineering Technical

 Conference, Sept.14-17,1997, Sacramento, CA, CD-ROM.
- [18] J.L. Lumley, Stochastic Tools in Turbulence. New York: Academic Press, 1970
- [19] J.L. Lumley, Atmospheric Turbulence and Radio Wave Propagation. Moscow: Nauka, 166-178, 1967

